Nonlinear multi-time-delay stochastic estimation: application to cavity shear layer and turbulent channel flow

Lasagna D.[a]
Engineering and the Environment, University of Southampton, Highfield, Southampton, SO17 1BJ

Fronges L.[b] and Orazi M.[c] and Iuso G. [d]
Dipartimento di Ingegneria Meccanica e Aerospaziale,

Politecnico di Torino, Corso Duca degli Abruzzi 24, Torino, Italia

A nonlinear extension of the multi-time-delay stochastic estimation technique is presented. The proposed approach consists in the design of nonlinear prediction filters based on Artificial Neural Networks or, for smaller problems, on Volterra expansions of the measured wall variable. The application to two different flows is discussed. The first case is the estimation of the temporal dynamics of the velocity fluctuations in a cavity shear layer in low subsonic conditions from wall-pressure measurements. The second case is the estimation of the streamwise velocity fluctuations in the buffer layer of a fully developed turbulent channel flow from wall shear stress measurements. It is shown that the accuracy of the nonlinear technique is application dependent, i.e. it is significantly affected by the underlying nonlinear nature of the flow investigated. In particular, we show that for the cavity shear layer case, the improvement is marginal and it does not appear to be worth the additional computational complexity associated with the nonlinear problem. On the other hand, the improvement in accuracy of the nonlinear estimation of the velocity fluctuations in the wall-turbulence case is significant, owing to the strong nonlinearity of the dynamics in the wall-bounded flow.

[a] Research Fellow, AIAA Member
[b] Master student
[c] PhD Student
[d] Full Professor

I. Nomenclature

a_i, b_{ij}, c_{ijk} = expansion coefficients

d = Taylor series truncation order

e = estimation error

E, $\mathbf{E}$ = conditional average event value,vector

h = half channel height, mm

L, W = cavity opening length and span, mm

n = number of past samples used for estimation

p = measured wall-pressure fluctuations, $\mathrm{N/m^2}$

Re_τ = Reynolds number based on friction velocity

s = measured wall variable or number of time lags

T_i = integral time scale, s

u = measured streamwise velocity fluctuation, m/s

u_τ = friction velocity, m/s

U_e = free stream velocity, m/s

Δt = sampling period, s

δ_0, θ_0 = boundary layer 99% thickness and momentum thickness, mm

ϵ = normalized mean square error

γ^2 = squared coherence function

Φ = power spectral density

ρ = correlation function

τ = longitudinal skin friction fluctuation, $\mathrm{N/m^2}$

Superscripts

$\bar{}$ = time average

$*$ = normalized fluctuation

$\tilde{}$ = conditional average

$\hat{}$ = estimated variable

$^+$ = quantity expressed in wall units

Subscripts

f = filtered fluctuation

II. Introduction

Today, achieving effective control of turbulent, separated and unsteady flows represents one major challenge for many aero-acoustics and aerospace applications. As it is well known, the potential benefits of active flow control are extensive and these motivate the large body of research being performed in this direction. As a multi-disciplinary area, active flow control also encompasses several interrelated aspects such as the description of coherent structures and the associated reduced-order models, before the control design can be undertaken. Nevertheless, one major challenge in this area is still the problem of obtaining an accurate estimation of the flow state for model-based control to be effective [1]. Therefore, active flow control is strictly interconnected to the understanding of the relationship between coherent structures and their signatures at the wall, measured by a small number of sensors for reasons of costs, complexity, data storage and processing time.

One technique, or better a class of techniques, which has been considered extensively in the fluids dynamics literature for these purposes is termed stochastic estimation. Stochastic estimation techniques were made popular by the early works of Adrian [2], where it was used to approximate conditional averages for turbulent flows. Stochastic estimation has now matured to become an established research tool that is able to provide valuable insight into the dynamics of coherent structures in free and wall-bounded flows, see Clark et al. [3] for recent perspectives on the topic.

Single-time-delay techniques, where information from only one time instant is used, were first introduced and applied extensively to a large class of flows. These techniques were then followed by the introduction of multi-time-delay approaches, where information from more than one time instant is used. Two approaches have been undertaken in this direction. The first operates entirely in the frequency domain and, therefore, it is called spectral linear stochastic estimation. It was introduced by Ewing and Citriniti [4] and has been developed in detail by Tinney et al. [5]. The second approach operates in the time domain, and was suggested by Ukeiley et al. [6] and later refined and studied in detail by Durgesh and Naughton [7] and Lasagna et al. [8]. Multi-time-delay techniques provide a more accurate representation of complex, unsteady flow fields, characterized by several convective time scales, and for systems operating in noisy environments. This last property essentially derives from the fact that multi-time-delay techniques are able to distinguish between

coherent and incoherent components, by implicit or explicit use of the squared coherence function.

These two techniques are linear, and they assume that the signatures of coherent structures in the flow field and at the wall are linearly correlated. However, this is not what has been observed for many classes of flows. One example is the relationship between the wall-pressure fluctuations beneath a turbulent boundary layer and dynamics of the coherent structures that populate it. Naguib et al. [9] used both linear and quadratic stochastic estimation and observed that the quadratic terms are required to obtain an accurate representation of the conditional velocity field. Similar conclusions were drawn by Ukeiley et al. [6], which used a complementary quadratic stochastic estimation/proper orthogonal decomposition, called modified quadratic stochastic estimation (mQSE), to elucidate the kinematic of the coherent structures in the shear layer of a compressible cavity flow. These authors also investigated the use of the linear spectral approach of Tinney et al. [5] on the same problem and found that the results were not as promising as using the mQSE approach. Hudy et al, [10], used both linear and quadratic single-time-delay stochastic estimation techniques to study the development of vorticity structures in a backward facing step flow, and found the nonlinear technique superior in reconstructing the details of the large scale structures. It appears clear that nonlinear approaches can highlight, quantify and capture relevant nonlinear features of the flow investigated, and can be therefore used as accurate observers for complex flows. A remarkable improvement appears to be the spectral high-order spectra analysis recently proposed by Baars et al. [11], which is based on a combination of proper orthogonal decomposition and high-order spectral analysis. The authors argue that the approach is able to identify the linear and nonlinear interactions in systems with multiple input and outputs, since high-order coherences are used. The authors applied the technique to an experimental data set of a coaxial axisymmetric jet at Mach=0.5, but found no quadratic noise propagation to the far-field of the jet. A different approach is the model-based nonlinear observer presented by Buffoni et al. [12]. Their method relies on the availability of a nonlinear low-dimensional Galerkin model of the flow and produces estimated time series of the modal coefficients that give the best approximation of the available measurements, while at the same time satisfying the dynamics of the reduced order model. However, the approach is meant to be applied off-line and it is not exactly suited for real-time applications.

The objective of this work is to present a nonlinear extension of the linear multi-time-delay technique, discussed in Lasagna et al. [8], and to critically analyze its advantages and disadvantages. We propose two different approaches to model the nonlinearity in the data: a feed-forward Artificial Neural Network and a Volterra series. Artificial Neural Networks have been employed in fluid mechanics problem in several contexts. For instance, ANNs have been used to develop black-box dynamical models as an alternative to the well-known Galerkin projection method, [13, 14], or for control design, [15, 16]. Application of Neural Networks for control of turbulent channel flow is discussed by Lee et al. [17]. Regarding flow estimation, Cohen et al. [18] designed a neural network based estimator for the flow past a circular cylinder in the laminar regime forced by vertical oscillations of the cylinder. The neural estimator used present and past velocity measurements from a few sensors located in the wake to predict the amplitudes of the first six modes obtained from Proper Orthogonal Decomposition of the cylinder flow. The estimator produced significantly better results than other techniques, owing, as suggested by the authors, both to the nonlinear nature of the estimator and to the inclusion of past measurements, which provided a dynamic estimation.

The technique discussed is compared with other existing methodologies, such as the linear multi-time-delay technique, and the classical linear and nonlinear single-time-delay techniques. To provide the validity for a larger range of characteristics we perform this comparison for two different flows. The first one is the problem of estimating the dynamics of the velocity fluctuations in a strongly resonating cavity shear layer flow, based on wall-pressure measurements. This case has been the subject of numerous investigations concerning stochastic estimation, see for example the works of Murray and Ukeiley [19] and Zhang and Naguib [20], and can be regarded as a benchmark problem. The second case investigated in this paper is the problem of estimating the velocity fluctuations in the near-wall region of a fully developed turbulent channel flow, based on measurements of the longitudinal wall shear stress. Stochastic estimation techniques have been previously applied to the problem of wall-bounded turbulence, for example the early work of Guezennec [21] and the work of Naguib et al. [9]. Since both these authors used single-time-delay stochastic estimation techniques, one additional objective of this work is to quantify and characterize the potential improvement of the multi-time-delay technique in the solution of the near-wall turbulence estimation problem. Various

other approaches have been proposed to tackle the problem of state estimation in wall-bounded flows, such as the work of Bewley and Protas [22], which used an adjoint-based algorithm using both pressure and skin friction measurements at the wall.

This paper is organized as follows. Section III briefly presents the mathematical framework of the nonlinear multi-time-delay technique and highlights a few relevant properties of the approach. Application of these techniques to the cavity shear layer and to the buffer layer is then presented in sections IV A and IV B, respectively. Finally, conclusions are offered in section V.

III. Mathematical background

To introduce the nonlinear multi-time-delay technique we consider the problem of estimating one velocity component u in a single point of the flow field, based on observations of the correlated variable s, pressure or shear stress, from a single sensor, located in some strategic point at the wall for practical reasons. Furthermore, because the mean value is known, or less interesting dynamically, all the quantities that we consider express the fluctuating component only. It is worth pointing out that the variable u can also represent the modal coefficient of a POD mode of a low-order nonlinear Galerkin model. The same procedure, replicated over all the modal coefficients of the model, would give a global reduced order estimate of the flow dynamics.

In order to compare different techniques, it is necessary to define an error metric that quantifies the estimation accuracy. The metric we use in this paper is the normalized mean-square error, defined as:

$$\epsilon = \frac{\overline{e(t)^2}}{\overline{u(t)^2}} = \frac{\overline{\big(u(t) - \hat{u}(t)\big)^2}}{\overline{u(t)^2}}. \tag{1}$$

where $e(t) = u(t) - \hat{u}(t)$ is the instantaneous deviation of the estimated quantity $\hat{u}(t)$ from the actual value $u(t)$, whereas the bar denotes temporal averaging over the time history.

At its core stochastic estimation provides approximations of the quantity $\tilde{u} = \langle u|E\rangle$, i.e. the conditional average of the fluctuations of u when the observed variable satisfies an event $E = \{s_E < s(t) < s_E + ds\}$, which confines it within a small window around the event mean value s_E. Approximations of the conditional average are usually expressed as a truncated Taylor series

expansion of the observed variable, in the form

$$\tilde{u}(t) \backsimeq \hat{u}(t) = \sum_{j=1}^{d} a_j s(t)^j, \tag{2}$$

where d defines the order of the expansion, and where the expansion coefficients can be easily obtained by straightforward application of the least squares technique, see reference [21] for a thorough explanation. The quantity $\hat{u}(t)$ can then be used to predict the flow state from wall measurements. This method is a *single-time-delay* approach since only one sample from $s(t)$, whether at the present time or in the past, i.e. $s(t-\tau)$, is used.

By contrast, in a *multi-time-delay* approach more than one sample is used. For control application purposes only present and past samples can be used, but this is not a necessary requirement for other situations. Furthermore, samples can be spaced equally back in time or can be taken at selected past time instants based on the occurrence of some specific condition, for example by tracking the peaks of the cross-correlation function. For the case where the samples are spaced uniformly in time, which is the case discussed in this paper, the multi-time-delay method corresponds to defining an expanded event vector $\mathbf{E}$ of the form

$$\mathbf{E} = \{s_0 < s(t) < s_0 + ds,\ s_1 < s(t-\Delta t) < s_1 + ds,\ \ldots,\ s_n < s(t-n\Delta t) < s_n + ds\}, \tag{3}$$

where Δt is the sampling period. This highly dimensional expanded event vector specifies a dynamic condition on the conditional average $\tilde{u} = \langle u|\mathbf{E}\rangle$ on $n+1$ simultaneous conditions and is able to capture in a better way the temporal dynamics of the flow, when n is adequately chosen.

From a general point of view, this conditional average can be written as a non-linear function f of the event elements, i.e. as

$$\tilde{u}(t) = f\big(s(t),\ s(t-\Delta t),\ s(t-2\Delta t),\ \ldots,\ s(t-n\Delta t)\big). \tag{4}$$

A linear approximation of f results in the linear multi-time-delay technique, where the estimate of the velocity is given by

$$\hat{u}(t) = \sum_{i=0}^{n} a_i s(t-i\Delta t) \tag{5}$$

and where the coefficients a_i can be first obtained off-line from a set of available measurements by use of the least squares procedure, and can then be used for real time estimation in online applications.

The linear approach might not be able to capture the full nonlinear complexity of the underlying relationship between the observed and estimated variables. This might be the case for certain strongly nonlinear physical processes, in which prediction of the flow state using nonlinear estimators might be required. In this paper we propose two different methods to find nonlinear approximation of the conditional average expressed by equation (4). The first method is a straightforward extension of the linear multi-time-delay technique and it is based on a Volterra series expansion, which is a common approach to model the response on nonlinear systems, in a wide range of research and engineering areas [23]. Essentially, the expansion contains a weighted sum of high-order products of present and past samples. For example, the expansion of order $d = 3$ has the form:

$$\hat{u}(t) = \sum_{i=0}^{n} a_i' s(t-i\Delta t) + \sum_{i=0}^{n}\sum_{j=i}^{n} b_{ij} s(t-i\Delta t)s(t-j\Delta t) + \sum_{i=0}^{n}\sum_{j=i}^{n}\sum_{k=j}^{n} c_{ijk} s(t-i\Delta t)s(t-j\Delta t)s(t-k\Delta t). \tag{6}$$

Note that the coefficients a_i are in general different from those of equation 5, hence the prime. The advantage of such a formulation is that it depends linearly on the expansion coefficients, and least squares techniques can be used to efficiently obtain a model out of data. However, the number of such coefficients can grow dramatically when nonlinear expansions of large orders are required to model strong nonlinearities, or when a large number of past samples has to be used, rendering the problem computationally expensive.

To cope with these issues, in this paper we also use Artificial Neural Networks (ANN) to model the nonlinear character of the conditional average expressed in equation (4). Artificial Neural Networks are computational models that can accurately approximate complex nonlinear input/output relationships with unknown structure. It is out of the scope of this paper to discuss the details and features of neural networks and the interested reader is referred to the book by Haykin, [24], or to the book by Hastie et al., [25], for a more statistics-oriented outline.

For the estimation problems discussed in this paper, we use standard feed-forward networks with a single hidden layer. This structure can represent to an arbitrary degree of accuracy any nonlinear function of the input, [24]. The networks have $n+1$ input nodes corresponding to present and past samples $[s(t),\ s(t-\Delta t),\ \ldots,\ s(t-n\Delta t)]$ of equation (4). These are densely connected to the n_h nodes in the hidden layer, which includes one bias node. Each hidden node includes a

nonlinear sigmoid activation function that modulates the weighted sum of the inputs. Finally, the hidden nodes are all connected to a single output node which provides, after the training process, a nonlinear estimate of $\tilde{u}(t)$. The connection weights between the nodes are the variables of an optimization problem. These are updated during the training process, which, as opposed to the Volterra series case, is a non-convex optimization problem, more difficult and lengthy to solve. The iterative Levemberg-Marquardt algorithm provided in the Neural Networks Matlab®Toolbox is used for this task.

An important aspect to discuss is the ability of an estimator to accurately predict the response on new independent data. Complex estimators with many tunable parameters and trained on small datasets may tend to fit the "noise" in the data and thus fail to capture the underlying trends, resulting in the so called *over-fitting*. In statistics, the difference between the *training* error, that is the error over the data which was used for the training, and the *validation* error, that is error on a new dataset, is often analyzed to assess the occurrence of such a problem. We refer the reader to Hastie et al, [25], for a thorough discussion of this problem and of different solutions. An interesting treatment of these issues in the context of flow state estimation is also given in the recent work of Clark et al., [3], where this issue is clearly demonstrated. For the two flows discussed in this paper, we have performed extensive preliminary tests for all the estimators presented. We have adopted a rather standard technique where the full dataset is first split into two parts of equal size. The estimator is obtained from the first block of data and the training ϵ_{tr} and validation ϵ_{val} errors are compared. The relative difference $1 - \epsilon_{tr}/\epsilon_{val}$ should be as small as possible for the estimator to be statistically accurate, whereas a large value indicates that the estimator will not generalize well to new data. Results of these analyzes will be discussed in the next section along with the other results. However, as a general comment, we have consistently observed that the relative difference between the training and validation errors was small enough to be indistinguishable from the uncertainty in the convergence of second order statistics of the data. This indicates that the estimators well describe the underlying behavior in the data and do not suffer of over-fitting. This is mainly due to the large size of the cavity and channel flow datasets, having 1.6 and 2 millions of samples, respectively. Furthermore, based on these observations we have then derived the estimators from

the entire dataset to achieve a further better convergence.

IV. Results

Results of application of the techniques introduced above for the two flows discussed are organized in two separate sections. In each section the problem and the experimental setup are briefly presented, followed by a preliminary data analysis to highlight the most important features of the flows, and by results obtained with the different estimation techniques.

A. Cavity shear layer

The first application presented in this paper is the estimation of the velocity fluctuations in the shear layer bounding a curvilinear cavity, based on wall-pressure measurements. This curvilinear geometry has been the subject of investigation by several researchers in the past few years, see for example references [26–28]. It was proposed as a device to control the flow past thick airfoils, to improve their aerodynamic performances by trapping a vortex inside of it. The problem treated in this paper is the same discussed by Lasagna et al. [8], where the linear multi-time-delay technique was discussed in detail. In this paper the nonlinear multi-time-delay technique will be applied to the same data set, to understand the role of nonlinearities in this resonating flow.

As schematically represented in figure 1, the pressure sensor is located under the cavity leading edge. In this paper we consider as a demonstrative example only the problem of estimating the velocity field at one characteristic point A in the shear layer. We selected the point where the largest velocity fluctuations have been measured, located at $y/\delta_0 = 1.73$ and $x/L = 0.58$, where δ_0 is the 99% thickness of the incoming laminar boundary layer, L is the cavity opening length and the coordinate system originates at the cavity leading edge. This point is representative of the dynamical features of the entire shear layer flow, which is dominated by intense oscillations.

1. Experimental setup

Referring to figure 1, the cavity model has a nominal opening length L equal to 68 mm, and a span W equal to 420 mm. The cavity model was embedded on the bottom wall of an open return wind tunnel facility, whose test section has width, height and length equal to 720, 300 and 3600

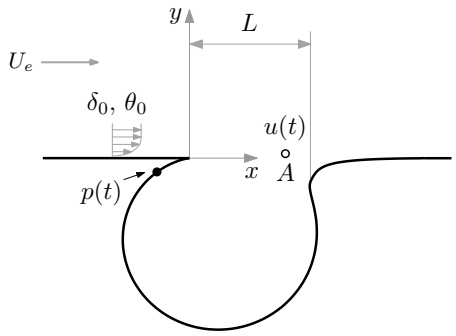

Fig. 1 Schematic representation of the cavity shear layer application.

mm, respectively. The free stream velocity U_e was set to 5.8 m/s, at which the Reynolds number based on the opening length was about 27700. The incoming boundary layer was laminar, and the ratio L/θ_0, where θ_0 is the momentum thickness at $x = -10$ mm, was equal to 113, that is high enough for the shear layer to develop self-sustained oscillations. Hot wire velocity measurements were performed across the whole shear layer using an A.A. LabSystems AN1003 anemometer with a built-in signal conditioning unit. A single-wire probe, (length 0.9 mm and diameter 5 μm), was used and it was frequently calibrated in situ in the middle of the vein. Wall-pressure measurements were performed with high-sensitivity electret condenser microphones, with diameter and height of 9.7 and 6 mm, respectively, positioned under the cavity model surface, below a 2 mm diameter hole. The microphones were calibrated with a high quality 1/4 in. Bruel&Kær (B&K) (type 4939) condenser microphone, using a frequency calibration procedure fully described in reference [8]. Velocity and pressure signals were sampled at 8.333 kHz by 24 bit resolution National-Instruments 9239 data acquisition modules, mounted on a NI cDAQ 9172 chassis. These units have a built-in anti-aliasing filter set at 46% of the sampling frequency. The sampling frequency is sufficiently high to accurately resolve all the relevant temporal scales of the flow, as it is more than fifty times larger than the fundamental oscillation frequency of the shear layer.

2. Preliminary analysis

In figure 2, the power spectral densities of the wall-pressure fluctuations Φ_{p^*}, panel (a), and of the velocity fluctuations at the control point Φ_{u^*}, panel (b), are reported. The two signals have been

normalized by their root-mean-square value, so that $u^* = u/u_{rms}$, $p^* = p/p_{rms}$. The power spectral densities in this plot, and the spectral quantities reported later in the text, have been computed using Welch's method, which improves the estimation error, by segmentation and averaging. Blocks with a length of 2^{13} samples have been used. A Hanning window is also applied on the chunks, before the Fourier transform, to reduce distortion of the spectral estimate due to side-lobe leakage, see for example Bendat & Piersol, [32].

The wall-pressure spectrum of figure 2-(a) is dominated by a very narrow band energy concentration at a fundamental frequency of 150 Hz. Furthermore, only the second and fourth harmonics of the fundamental frequency, at 300 and 600 Hz, are clearly distinguishable in the plot. In addition, the pressure spectrum shows a multitude of other spectral peaks and broadband components, which can be attributed in part to physical features of the cavity flow, e.g. the recirculating flow, turbulent structures convected along the cavity wall, and in part to colored background noise originated by the facility. It is clear that from a practical point of view, robustness to noise is of paramount importance for any estimation technique, where the goal is to effectively separate the relevant information from incoherent noise.

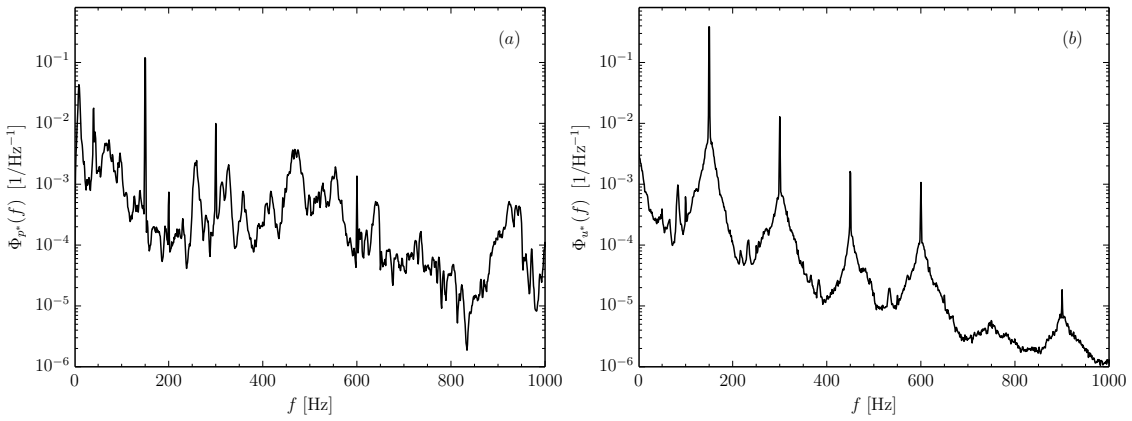

Fig. 2 Power spectral densities of the normalized wall-pressure and velocity signals, in panels (a) and (b), respectively.

On the other hand, the frequency spectrum of the velocity fluctuations, figure 2-(b), shows a remarkable difference with respect to that of the wall-pressure fluctuations. The spectrum is still dominated by the peak at the fundamental frequency, but, as opposed to the wall-pressure spectrum,

all the harmonics are clearly distinguishable and feature prominently in the velocity signal.

We want to stress that in order to accurately reconstruct the velocity signal, all the harmonics have to be reconstructed, although it is clear that most of the energy in the signal, i.e. most of the dynamics in the velocity field, is contained in the first mode at $f_{wt} = 150$ Hz.

It has to be noticed that the two spectral distributions are partially originated by a weak acoustic resonance of the wind tunnel settling chamber. The resonance generates a coherent pressure perturbation across the entire facility at the fundamental frequency $f_{wt} = 150$ Hz. Although relatively weak, the pressure perturbation is sufficiently intense to make the shear layer flow lock onto it. As a result, the velocity field develops very coherent fluctuations, while at the same time the pressure fluctuations in the cavity region are amplified by the Kelvin-Helmholtz instability. A similar response of an open cavity flow has been previously noticed and studied in detail, for example by Chatellier et al. [29] and by Sipp [30].

To gain more insight into the relationship between the wall-pressure and the velocity, figure 3 shows the squared coherence function γ^2_{up}, defined as:

$$\gamma^2_{up}(f) = \frac{|\Phi_{up}(f)|^2}{\Phi_u(f)\Phi_p(f)} \tag{7}$$

where Φ_{up} is the cross-spectral density of the velocity and wall-pressure signals. The squared coherence function expresses the level of linear correlation between two variables in the frequency domain, and highlights where relevant information lies in the signal of the measured variable.

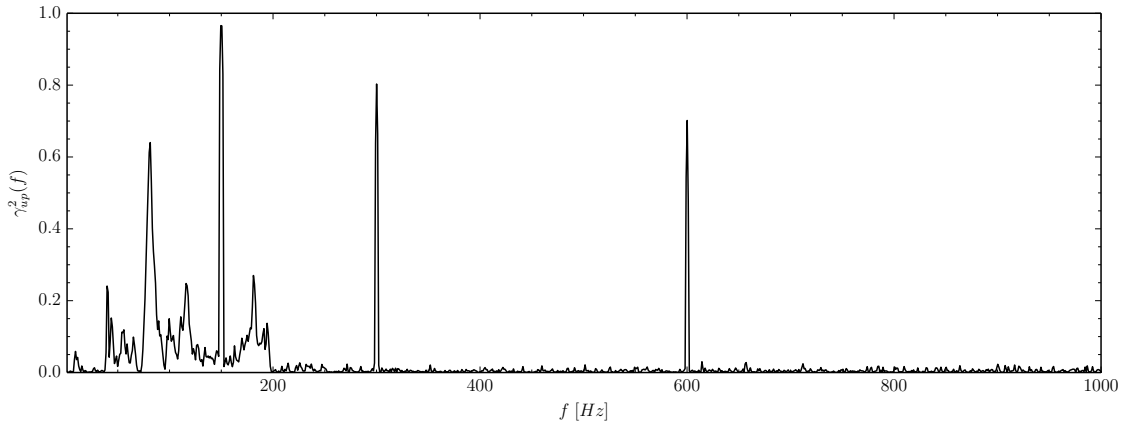

Fig. 3 Squared coherence function of the joint velocity and wall-pressure fluctuations.

The main feature of the plot is that the level of coherence is very high only at the acoustic

resonance frequency and at its first two harmonics, i.e. at 150, 300 and 600 Hz. At higher frequencies the only remaining feature is a weak coherence peak at 1200, but it is omitted from the plot because the corresponding energy in the velocity signal spectrum, figure 2-(b), is much weaker than the peak at the fundamental frequency, which dominates the shear layer motion. We also observe that there is a fair level of coherence at frequencies in the range 30-200 Hz, which can be attributed to physical phenomena of the cavity flow considered here, such as the recirculating flow inside the cell and to sub harmonics of the fundamental frequency, at 75 and 32.5 Hz. Outside of this range the coherence between the velocity and pressure signals is practically zero, and most importantly it is zero at integer multiples of the fundamental resonance frequency which do not belong to the harmonic series $f_i = 2^i f_{wt}$.

It is clear from this preliminary analysis that most, if not all, of the useful information is contained in few selected frequencies. Other components in the band 30-200 Hz, with non negligible coherence levels, have a limited energetic content. In addition, the vast difference in spectral features of the two signals poses a significant challenge to the estimation problem, because of the large amount of uncorrelated components that lie in the pressure measurements. These flow field characteristics suggest that pre-filtering the pressure signal, to separate the "signal" and "noise" components, might simplify the estimation problem. This approach is discussed in section IV A 4, but for the sake of clarity, it is preceded by results obtained with the full pressure signal, reported in section IV A 3.

3. Linear and nonlinear multi-time-delay techniques with full pressure signal

In figure 4 we report the behavior of the normalized mean-square error, defined in equation (1) of the estimated velocity fluctuations using the linear multi-time-delay technique, solid line, as a function of n, while the cross symbol refers to estimation results obtained using a nonlinear multi-time-delay technique, at $n = 200$. This nonlinear estimation was obtained by using an Artificial Neural Network, having 201 input nodes, corresponding to the 201 samples of the pressure signal, 40 hidden nodes to represent the nonlinearity, and one output node for the estimated velocity. Because of the large computational time required to train this network, due to the large size of the available data set and to the complexity of the network architecture required by the high number of input

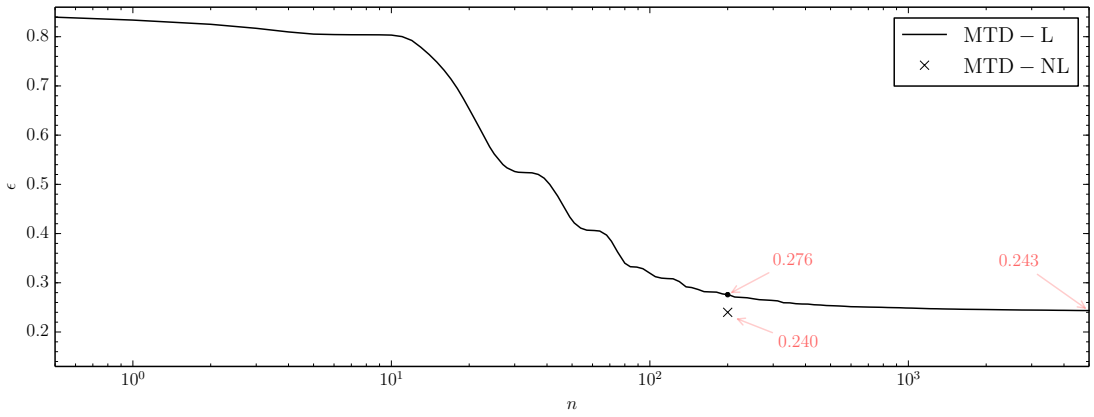

Fig. 4 Normalized mean-square estimation error of the velocity fluctuations as a function of n, for linear, (MTD-L), and nonlinear, (MTD-NL), multi-time-delay analyzes. For the nonlinear case, only the point at $n = 200$ is shown.

nodes, we decided to perform the computations only for $n = 200$, as a compromise between the computational time and the significance of the result with respect to the linear case.

From the plot, and concerning the results of the linear technique, we observed that the number of past samples required to achieve a consistent reduction of the estimation error is very large and it is on the order of hundreds of samples. In particular, the normalized error decreases from 0.840 for $n = 0$, which corresponds to the classical linear stochastic estimation to 0.243, for $n = 5000$. This result clearly shows that a dynamic estimator is required to faithfully capture the shear layer temporal evolution. More detailed theoretical motivations regarding these results are provided in our previous work, in reference [8].

For the nonlinear estimation approach, we observed that the improvement in accuracy with respect to the linear technique is marginal, since the normalized error has decreased from 0.276 to 0.240 for $n = 200$. Hence, in the present experiment, the nonlinearity between the shear layer velocities and the wall-pressure fluctuations appears negligible, at least from the point of view of the reconstruction error. It may be argued that this result is due to the fact that the amplitude of the velocity and pressure fluctuations are both mostly driven by the acoustic resonance of the facility, rather than by a pure feedback loop. Hence, it would be of interest to investigate this speculation further on other datasets. In fact, several other researchers which investigated estimation of cavity

flows from wall-pressure measurements have shown that nonlinear techniques produce a significant improvement in accuracy, e.g Murray et al., [19]. A nonlinear estimator, and more precisely the quadratic stochastic estimation, was also successfully employed by Samimy et al., [31], to estimate the amplitudes of Proper Orthogonal Decomposition modes in a feedback control experiment on subsonic cavity flows.

It is important to point out that the curve for the linear estimator, which shows the training error on the entire dataset, exhibits a rather flat plateau for large values of n, as opposed to what has been observed by other researchers, see for example references [7] and [3]. In these works, as the number of past samples in increased, the training error decreased monotonically, whereas the error on an independent validation set started to increase. Hence, the relative difference between the two errors increased as well, and the estimator did not correctly describe anymore the general trends in the data. For our results in figure 4, and regarding the linear case, the relative difference between the training and validation errors is within $1/400$ at $n = 5000$, which is already quite beyond the value of n that one would select for practical use from the plot of figure 4. For the nonlinear estimator, at $n = 200$, the relative difference is less than $1/200$. These values show that the results of figure 4 are statistically accurate and are not affected by a significant over-fit.

Despite the slight improvement in the value of the mean-square error given by the nonlinear technique, the spectral properties of the estimated velocity fluctuations are strongly affected. Power spectral densities of the measured and estimated velocity signals are shown in figure 5. Spectra for the linear and nonlinear multi-time-delay techniques discussed above are presented for comparison, where for both methods $n = 200$. Furthermore, in order to highlight the details of the reconstruction of the spectra at the peak frequencies, the peaks have been marked with a horizontal segment, centered on the peak for the measured velocity signal, shifted on the left for the linear technique and on the right for the nonlinear technique. The numbers on top of each segment indicate the fraction of reconstructed energy contained in a frequency band of width 1 Hz around the peak frequency. We observe that the slight improvement in accuracy of the nonlinear estimation presented in figure 4 is essentially due to a slightly better reconstruction of the energy at the fundamental frequency. However, the peak energy is already quite correctly reproduced by the linear estimate.

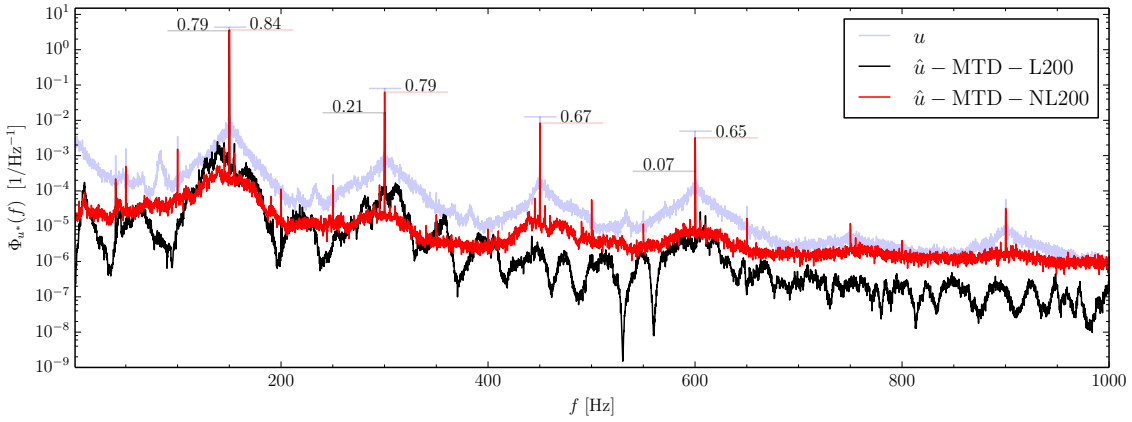

Fig. 5 Measured and estimated power spectral densities of the normalized velocity fluctuations. Spectra have been reconstructed using both linear, MTD-L200, and nonlinear, MTD-NL200, multi-time-delay analyzes, with $n = 200$. Horizontal segments indicate the peak height, and the numbers represent the fraction of energy recovered at the peak position, for the linear technique on the left of the peak, and for the nonlinear technique on the right.

The slight reduction in estimation error is also partly due to a more efficient recover of the energy of the harmonics, which however have a relatively low energy in the measured signal compared to the fundamental frequency. In particular, we observe that the nonlinear technique is able to reconstruct the dynamics quite well at a frequency equal to 450 Hz, where the linear technique fails completely. This is due to the fact that there is no coherence at this frequency between the velocity and pressure fluctuations and the linear multi-time-delay technique filters this component out as if it was incoherent. This is a fundamental and interesting property of the nonlinear technique which will be discussed extensively in the rest of the paper.

4. Pre-filtering of the pressure signal

It has been shown in the previous section that a very large number of past samples have to be used to recover the essential information in the velocity signal. However, this is in clear contrast to the fact that the relevant dynamics are, at least for a linear approach, contained in few distinct frequencies. Thus, loosely speaking, the number of degrees of freedom required to model these dynamical features and to accurately recover the velocity field, should be small. Furthermore,

as mentioned in the previous section, the complexity of the solution of the nonlinear estimation problem increases dramatically with the number of past samples and more compact systems should be preferred. To cope with these issues we adopted an approach based on pre-filtering the pressure signal to eliminate all those frequency components that do not carry useful information for estimating the velocity field. Here, we assume these components are those for which the squared coherence function of figure 3 is low. Therefore, we decided to retain in the wall-pressure signal the fundamental frequency f_{wt} and the two harmonics at $f = 300$ Hz and $f = 600$ Hz. The components in the band between 30 and 200, are also filtered out of the signal with the exception of the fundamental frequency. This choice was adopted because the spectrum of the velocity signal indicates low energies at these frequencies, and they do not appear to contribute significantly to the dynamics of the shear layer.

For maximum effectiveness, the filtering is done off-line by setting the Fourier coefficients of the transform of the signal corresponding to frequencies out of a narrow band wide 1 Hz around the selected frequencies to zero, and taking the inverse transform to recover the data in physical space. The choice of the band width can be justified by the sudden drop of energy around the peak. In the following the filtered pressure will be denoted with the symbol p_f.

a. Single-time-delay techniques We introduce the results for classical single-time-delay estimation with a discussion of the joint probability density function. For classical single-time-delay stochastic estimation, which aims at approximating conditional averages, the joint probability density function is a quantity of interest. Traditionally, [33], it is recognized that when the distributions of the data and of the event are not jointly normal, some kind of non-linearity must be taken into account. As a consequence, examination of the JPDF can readily highlight the need for inclusion of quadratic or high-order terms.

We report in figure 6 the normalized joint probability density function (JPDF), panel (d), and the PDFs, in panels (e) and (b) for the normalized velocity signal u^* and the normalized pressure signal p_f^*, respectively. Furthermore, in figure 6-(d), the conditional average of the velocity fluctuations are reported for seven equally spaced events, defined when the pressure fluctuation p_f^* lies within a window of size $\delta p_f^* = 0.1$. The error bars around the conditional average data indicate

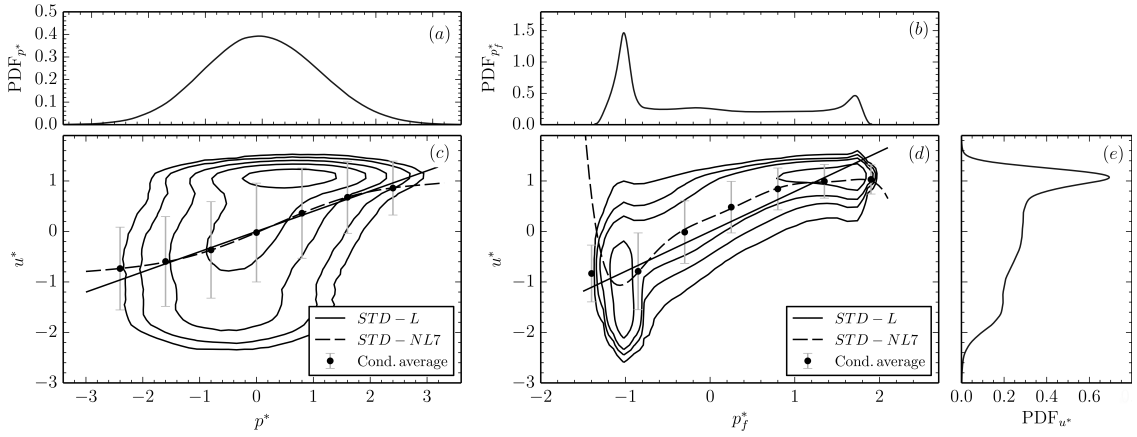

Fig. 6 Contour lines of the joint probability density function of the filtered wall-pressure fluctuations and velocity fluctuations, (d) **. Probability density functions of the velocity,** (e)**, and filtered wall-pressure,** (b)**, fluctuations. Panel** (c) **shows the JPDF of the velocity and full wall-pressure fluctuations, whereas panel** (a) **shows the PDF the full wall-pressure fluctuations.**

the conditional root-mean-square value of the velocity fluctuations, which essentially denotes the uncertainty associated with the conditional average estimate and in ultimate analysis of the nonlinear single-time-delay technique. In addition, linear and nonlinear 7^{th} order single-time-delay stochastic estimates are also shown. The seventh order was chosen since the mean square error does not decrease anymore if the expansion order in equation (2) is increased further.

For the sake of reference, in panel (c) of the same figure we reported the JPDF of the velocity and pressure fluctuations before the pre-filtering step, together with the corresponding conditional average data, (with same window size), and linear and nonlinear stochastic estimates. In addition, in panel (a) the PDF of the full pressure signal is reported. Note that the horizontal scale of panels (d) and (c) is not the same, since the filtered signal fluctuations have a variance which is about 25% of the corresponding value for the full signal.

Considering the case where the pressure signal has been filtered, we observe that the contours of the JPDF are very distorted, strongly non-Gaussian and significantly more compact around the conditional average with respect to those of the unfiltered pressure signal. Clearly, by removing the incoherent components the underlying behavior of the data has appeared. As a result, the conditional average is able to represent much better the velocity fluctuations. This is evident,

d	1	2	3	4	5	6	7
$\epsilon_{filtered}$	0.377	0.341	0.339	0.334	0.329	0.325	0.325
ϵ_{full}	0.840	0.839	0.837	0.837	0.837	0.837	0.837

Table 1 Mean-square estimation error of the velocity fluctuations as a function of the order of the Taylor expansion for single-time-delay linear and nonlinear stochastic estimations. The first row refers to results obtained with the filtered wall-pressure signal, while the second row refers to the unfiltered signal case.

qualitatively, from the reduced length of the error bars around the conditional average for the filtered signal.

The conditional average data expresses a significant nonlinearity in the signals, which is now captured more accurately by a highly nonlinear interpolation, than with a pure linear approach. This feature is clearly reflected in quantitative terms by the value of the normalized mean-square error, reported in table 1, which shows the normalized mean-square estimation error for expansion orders d between one and seven. In the table, the first row reports the values of ϵ corresponding to the filtered wall-pressure signal, while, for comparison, the second row reports the corresponding values for the full pressure signal. We first observe a general decrease of the value of ϵ for the filtered signal. This is due to the fact that, unless many sensors are used, single-time-delay techniques are not able to cope with noisy signals, which cause a significant degradation of the accuracy. Such a feature suggests that for classical single-time-delay techniques it is crucial to have data of the measured variable, wall-pressure in the present case, which is as clean and accurate as possible because noise enters directly into the estimation process. Furthermore, we also observe a reduction of error when the expansion order is increased, as opposed to what can be observed with the full noisy pressure signals, where no appreciable improvement is noticed.

The PDF of the filtered pressure fluctuations, figure 6-(b), is significantly different from that of unfiltered signal, in panel (a), where the distribution is close to being Gaussian. This is because most of the background "noise" contaminating the wall-pressure signal has been removed and the underlying "signal" part has emerged, evidencing two peaks resulting from the oscillatory nature of the signal.

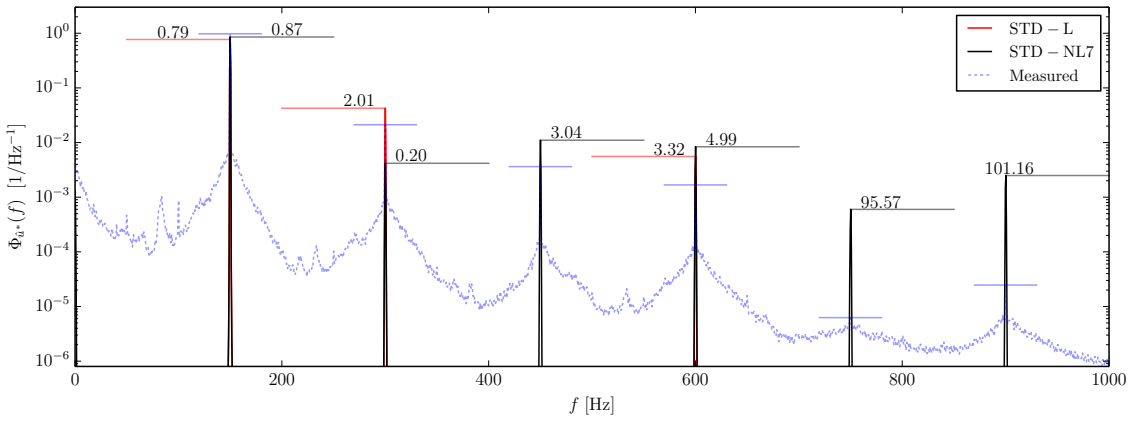

Fig. 7 Power spectral densities of the reconstructed velocity signals $\hat{u}^*$ for the linear and nonlinear single-time-delay techniques. The thin blue curve is the spectral density of the measured velocity signal. The horizontal segments define the height of the peaks of the spectra, while the numbers indicate the fraction of energy recovered.

In order to gain insight into why the nonlinear technique results in a lower error, we report in figure 7 the spectra of the reconstructed velocity signals using a linear and a nonlinear seventh order single-time-delay stochastic estimation techniques, denoted STD − L and STD − NL7, respectively. To enhance the readability of the plot, the peaks have been marked by small horizontal segments, and the numbers represent the fraction of energy recovered, on the left/right of the peak for the linear/nonlinear technique. In addition, the spectrum of the measured signal is also shown and the peaks are denoted by shorter horizontal segments.

It can be observed that the linear and nonlinear techniques produce roughly the same results at the fundamental frequency $f = 150$ Hz, since they recover 79% and 87% of the energy of the fluctuations at that frequency.

An interesting feature occurs at $f = 450$ Hz. In fact, we observe that the linear case does not recover energy at this frequency, since it is not present in the filtered pressure signal, hence there is no number on the left of this peak. On the other hand, the nonlinear technique produces a strong peak at this frequency. This occurs because the nonlinear filtering operation produces all the integer multiples of the fundamental frequency. Nevertheless, the energy at this frequency is over-estimated and is a source of error for the nonlinear technique.

At $f = 600$ Hz, both techniques produce a large error, and they significantly over-estimate the energy of the fluctuations at this frequency. For the linear case, this is due to the fact that the value of the coefficient of the Taylor expansion of equation 2 is, for this case, determined mainly by the properties of the signal at the fundamental frequency, which energetically dominates the fluctuations and the auto- and cross-correlation functions. In the frequency domain, the transfer function corresponding to the linear single-time-delay technique has a constant gain. Thus, the height of the peaks of the reconstructed signal at all the other frequencies is essentially driven by one single coefficient and energy can be significantly over-estimated. For the nonlinear case, this features does not hold exactly because the transfer function concept does not apply, but the principle is similar. In fact, we observe that the energy at frequencies 750 and 900 Hz is significantly over-estimated. This drawback of classical single-time-delay estimates is what makes multi-time-delay techniques interesting, because each frequency component can be adjusted in both phase and amplitude as required to achieve a minimum mean-square error [8].

b. Multi-time-delay techniques Figure 8 shows the behavior of ϵ as a function of n, for Volterra series expansion orders d equal to 1, linear multi-time-delay technique, and for orders 2 and 3, nonlinear multi-time-delay technique. Let us first consider the results for the linear case. We observe that the number of past samples at which ϵ reaches a plateau value has decreased from hundreds, when the full pressure signal is used, to about five, beyond which no further increase in accuracy can be gained by increasing n. This is a remarkable result, which provides a dramatic simplification of the estimation problem, to the point where a Volterra model could be derived. Note that the asymptotic value of ϵ obtained with the filtered pressure signal is just slightly larger than what can be obtained with the full pressure signal, i.e. 0.240, which contains all the available information. This is due to the fact that despite some information was discarded by filtering the pressure signal, most of the relevant information to estimate the velocity fluctuations is still contained in the filtered time history.

The reason why the number of required past samples has drastically decreased can be better understood in the frequency domain. It is known that the linear multi-time-delay technique is an optimal Finite Impulse Response Wiener prediction filter, which produces a reconstruction of the

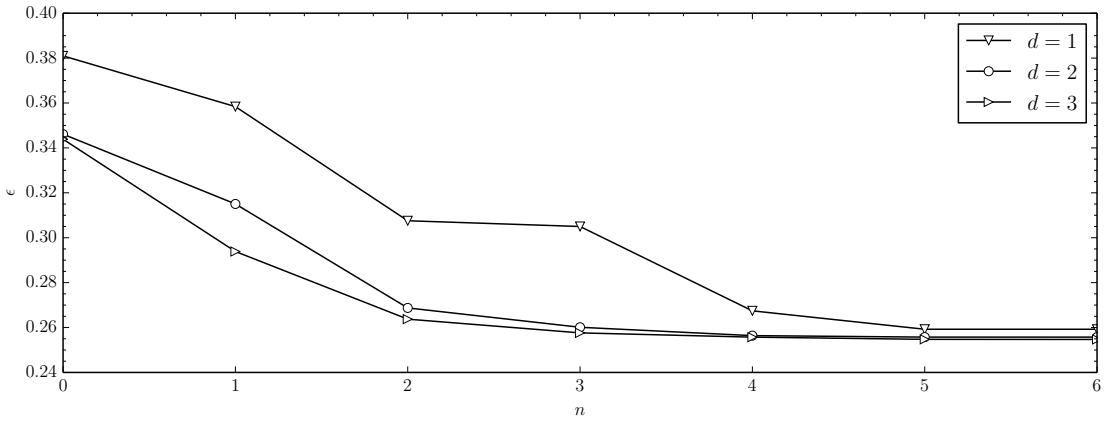

Fig. 8 Normalized mean-square error of the estimated velocity fluctuations, as a function of n, and for a linear, $d = 1$, and non-linear, $d = 2, 3$, Volterra expansions.

velocity fluctuations with minimum mean-square error. In the spectral domain, a transfer function corresponding to this filter can be introduced. The effect of the transfer function is to filter incoherent components, while retaining the coherent part, by amplifying and phase-shifting each frequency component as required to achieve the minimum estimation error [8]. The required complexity of the transfer function, which ultimately determines the required number of past samples, depends on the complexity of the signals and on their frequency domain properties. Therefore, a possible explanation for our results is that, on the one hand, when the pressure signal is filtered, there are only three distinct frequency components which have to be adjusted in both amplitude and phase. On the other hand, with the full signal, the complexity of the transfer function has to be much higher because of the high number of zeros needed to amplify the important frequencies only and to filter out all the remaining components.

Due to this dramatic reduction in complexity, and because the required number of past samples is significantly reduced, a full nonlinear Volterra expansion of the event vector can be performed, instead of resorting to neural networks. In figure 8, we observe that for low values of n the nonlinear technique is more accurate than the linear technique, even though the improvement brought by the cubic expansion is less noticeable than what can be obtain increasing d from 1 to 2. Nevertheless, the fundamental result is that the asymptotic value of the error obtained by the nonlinear technique is only slightly lower than what can be obtained by the less complex linear approach. In fact, for

$n = 6$, ϵ decreases from 0.254 for $d = 1$ to 0.250 for $d = 3$. This result appears similar to what could be observed in figure 4, where the nonlinear approach was only slightly more accurate than the linear technique.

Crucially, this means that to faithfully reconstruct the energy of the shear layer fluctuations, at least at the control point and from the standpoint of the reconstruction error only, a linear technique is sufficient for the current dataset. In addition, the complexity of the design of the nonlinear filter is significantly increased, as well as its implementation on a real-time hardware in a physical experiment where an estimate of the flow state is required.

It is worth investigating the spectral characteristics of the signal reconstructed using the nonlinear multi-time-delay techniques. To this end we report in figure 9 the power spectral densities of the estimated velocity fluctuations using Volterra expansion order $d = 1,\ 2,\ 3$, in panels (a), (b) and (c), respectively, for $n = 6$. In each plot, the spectrum of the measured velocity fluctuations is reported in light blue, while the estimated spectra are reported in black. Furthermore, the thin horizontal segments indicate the peak levels of the measured and reconstructed spectra, while the number reports the fraction of energy reconstructed by each technique at the peak frequency only. We first observe that since the wall-pressure signal has been pre-filtered by completely removing those frequency components at which the squared coherence was low, the reconstructed spectra only show non-zero energy at those frequencies, and at their integer multiples for the nonlinear techniques. In panel (a), for the linear expansion, we only observe three peaks, at $f = 150,\ 300$ and 600 Hz. This is because the linear multi-time-delay technique only amplifies and shifts frequency components which are already present in the signal. By contrast, in the spectra of the velocity fluctuations reconstructed with nonlinear expansions we observe a multitude of peaks, at all the integer multiples of the fundamental resonant frequency, similarly to what was discussed for figure 7. The reconstruction error for all the peaks decreases by using estimation techniques of increasing expansion order. For instance, we observe that the quadratic and the cubic expansions are able to recover a large fraction of the energy corresponding to the third peak, at $f = 450$ Hz, while no reconstruction at all is done by the linear technique.

This is a fundamental frequency domain property of the proposed nonlinear approach. In addi-

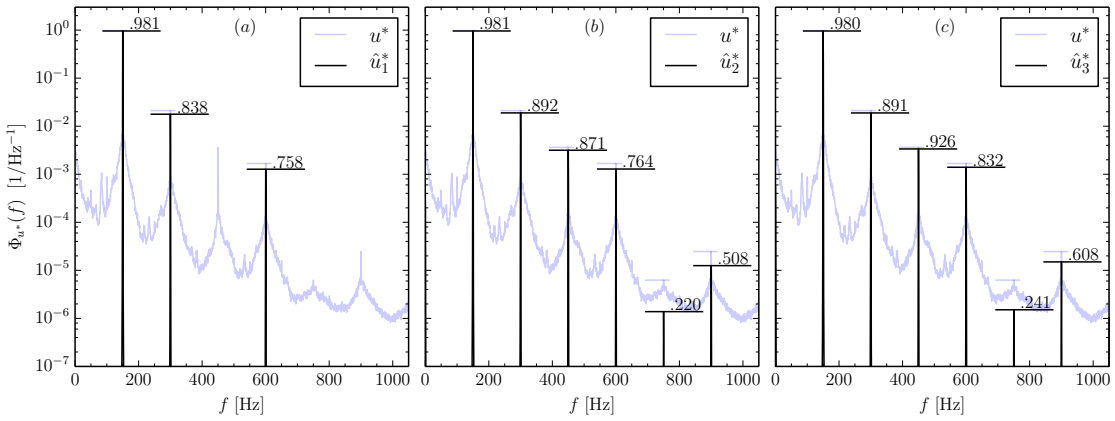

Fig. 9 Measured (light blue) and estimated (black) power spectral densities of the velocity fluctuations at the control point for a linear, (a), quadratic, (b), and cubic, (c), stochastic estimation techniques. Results concern the filtered wall-pressure signal. The horizontal segments define the height of the peaks of the spectra, while the numbers indicate the fraction of energy recovered.

tion, it is worth pointing out that when two or more sine waves exist in the signal at discrete frequencies f_a and f_b, a nonlinear filtering operation excites energy by inter-modulation at $f = k_a f_a + k_b f_b$, where k_a and k_b are positive or negative integer numbers. This feature enables a nonlinear estimation technique to reconstruct complex nonlinear couplings and interactions that may be present in the flow being investigated, which may not be captured by a purely linear approach.

B. Turbulent channel flow at $Re_\tau = 180$

The second application discussed in this paper is the estimation of the velocity fluctuations in wall-bounded turbulent flow based on measurements of the longitudinal skin friction at the wall. State estimation in wall bounded turbulent flow is a fundamentally different problem with respect to the narrow-band, resonating cavity shear layer case. The complex dynamics of the coherent structures and their signature at the wall define a significantly more challenging task for the estimator, which should take into account a much large number of spatial and temporal scales.

As a benchmark problem to assess the capabilities of the techniques discussed in this paper, we consider the fully developed incompressible turbulent flow in a channel, at a skin-friction based Reynolds number $Re_\tau = u_\tau h/\nu$ equal to 180, where h is the half channel height, u_τ is the friction

velocity and ν is the kinematic viscosity. In addition, we concern ourselves exclusively with the problem of estimating the amplitude of the streamwise velocity fluctuation only, and at a few selected and representative distances from the wall, at the same streamwise and spanwise position of the wall-mounted shear stress sensor.

For this task, we first selected a location in the viscous sublayer at $y^+ = 5$, where strong linearity between the velocity fluctuations and the shear stress at the wall is expected. The second location is at $y^+ = 12$, in the buffer layer. This location is chosen because the buffer layer is the region of a wall bounded turbulent flow where most of the relevant physics of near wall turbulence take place, such as the dynamics governing the wall turbulence regeneration mechanisms [34]. The velocity fluctuations and the wall shear stress are consequently strongly influenced by the interaction between the coherent structures and the intense shear motions populating the near wall region. From this standpoint, reliable and accurate estimation of the near-wall dynamics is deemed an important milestone, especially when feedback control of wall turbulence is of ultimate interest, e.g. Colburn et al.,[1]. The third location chosen is at $y^+ = 50$. Essentially, this location was chosen because it lies in the logarithmic region. Although the estimation of the flow state in these regions is not crucial for feedback control systems, it represents a challenging benchmark problem for the stochastic techniques presented and discussed in the present paper.

1. Experimental setup and definitions

Experimental data were obtained in a previous control experiment of wall bounded turbulence in a channel flow [35], which the reader is referred to for a full description of the experimental setup and the conditions. The half channel height h is equal to 10 mm and the span of the test section is such that the aspect ratio width/height is equal to 14. The total length of the facility is 8 m. Measurements of velocity and shear stress were performed at $x = 6$ m, which is about $600h$ from the inlet section and $200h$ from the exit section, guaranteeing a fully developed turbulent velocity profile while reducing to the minimum the interference with the end sections of the facility. Simultaneous measurements of the wall shear stress and of the streamwise velocity were performed at the same streamwise and spanwise location with an ad hoc hot wire shear stress probe and a single sensor hot

wire velocity probe, respectively. Both sensors are based on a 1.2 mm long ($l^+ = 22$), 5 μm diameter tungsten-platinum wire. The hot wire probe is calibrated in situ against the pressure differential on the contraction section of the channel facility while the shear stress sensor is calibrated using the longitudinal mean pressure gradient on the channel, measured by a set of static pressure taps located along the facility. A Dantec 55M01 high precision CTA anemometer is used, with overheating ratio equal to 1.8. Time histories of 2^{20} samples were acquired simultaneously for the velocity and shear stress at a sampling frequency $f_s = 12$ kHz, corresponding to 0.4 viscous time units, using a 16 bit PCI-MIO-16-XE board. In the following, the symbols u and τ will be used to denote the fluctuating component of the velocity and wall shear stress signals.

2. Preliminary analysis

An estimate of the temporal integral scale of the dynamics of the dominant coherent structures in the turbulent near-wall flow can be inferred from the analysis of the normalized auto-correlation function of the velocity and shear stress fluctuations. As common practice, the definition of the auto-correlation function for some generic variable f that we use in this paper is

$$\rho_{ff}(s\Delta t) = \frac{\overline{f(t)f(t+s\Delta t)}}{\overline{f(t)^2}} \tag{8}$$

where the bar denotes a temporal arithmetic average.

The evaluation of the integral time scale T_i, based on numerical integration of $\rho_{uu}(s\Delta t)$ from $s = 0$ to s where ρ_{uu} is first equal to or less than 10^{-2}, produces an approximate duration of the characteristic near-wall structures defining the appropriate time scales to be used in the multi-time approach. In units of samples, T_i is equal to 42, 45 and 32 for the velocity fluctuations at $y^+ = 5$, 12 and 50 respectively, while it sets to 48 lags for the wall shear stress. In terms of viscous units, the values become 16.9, 18.3 and 13.1 for the velocity fluctuations and 19.5 for the shear stress.

It can be argued that information contained in the measurements of the wall quantity, which can be used to predict the state of the flow at some given instant, lies in a window having approximately the size of the integral scale. Furthermore, if the local mean convective velocity is taken into consideration, these integral scales also provide an approximate indication of the streamwise length

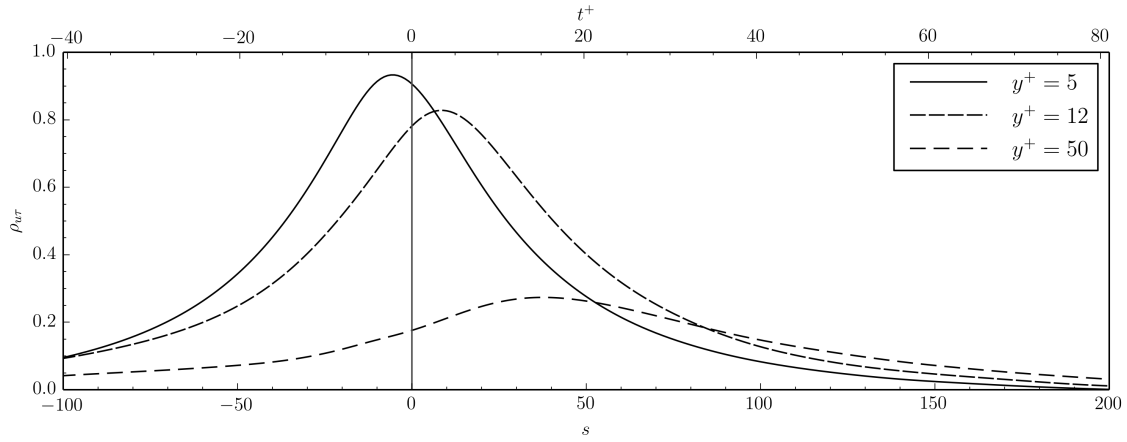

Fig. 10 Cross-correlation functions of the velocity and wall shear stress fluctuations, as a function of the lag, s, for the three distances from the wall. For clarity, the lag is also expressed in viscous time units, by the top x-scale.

of the region within which accurate estimates could be produced.

A fundamental quantity that drives the estimation results is the cross-correlation function between the velocity and shear stress fluctuations, which succinctly defines the quality and reliability of the signatures of the coherent structures at the wall. The cross-correlation function, defined as

$$\rho_{u\tau}(s\Delta t) = \frac{\overline{u(t)\tau(t+s\Delta t)}}{\overline{u(t)^2}^{1/2}\overline{\tau(t)^2}^{1/2}}, \tag{9}$$

is reported in figure 10 for the three distances from the wall. In the figure, the horizontal scale has been reported both in terms of the number of lags s, on the bottom, to emphasize the results reported in the next sections, where the focus is on the number of past samples included in the multi-time-delay estimate, and in viscous time units, on the top.

As expected from the physics and from the stochastic nature of the fluctuations in the near-wall flow, we observed high levels of cross-correlation between u and τ in the near-wall region, at $y^+ = 5$ and 12, whereas lower, but still significant, correlation levels were measured for a distance farther from the wall, at $y^+ = 50$.

The lag $s_{\rho_{max}}$ for which the velocity and shear stress time histories are most correlated also changes with the distance from the wall. In particular, the sign of $s_{\rho_{max}}$ is negative from $y^+ = 5$, whereas is becomes positive for $y^+ = 12$ and 50, and eventually also increases in amplitude with the distance from the wall. The sign of $s_{\rho_{max}}$ depends on the relative streamwise position of the

shear stress probe and the point where flow estimation is of interest. In the present experiment, where the two probes are located at the same streamwise coordinate, if the sign is positive, then on average the coherent structures in the buffer layer are first detected by the hot wire velocity probe but their signature is captured by the shear stress sensor after a short interval.

This interpretation is in agreement, especially for the buffer layer case at $y^+ = 12$, with the established knowledge about coherent structures in wall bounded flows, e.g. see references [34, 36], where quasi-streamwise vortices very near the wall are tilted with respect to the mean flow direction. Thus the "heads" of the vortices, located in the buffer layer, arrive at the velocity sensor before their "tails" are revealed by the shear stress sensor.

Because of the inherent convective characteristics of the wall-bounded flow considered here, where the relevant information arrives on the shear stress sensor with some delay, it is not possible to accurately predict the flow evolution above the sensor, essentially because future samples of the wall shear stress would be required, rendering the problem partially non-causal. To circumvent this issue, in the present paper we adopt a shifting technique, discussed later in the paper, whereby the time history of the wall shear stress is shifted appropriately in time. Of course, in a physical experiment this approach would not be feasible, but it is evident that the shear stress probe would be placed upstream of the region where estimation is required, and such that the relevant information on the dominant flow structures can be detected in time.

In the frequency domain, the squared coherence function defined in equation (7) provides a frequency dependent measure of the information content in the measurements of the wall variable.

In figure 11 the squared coherence function of the joint velocity-shear stress fluctuations is shown, for the three distances from the wall. The top x-axis scale reports the period T^+, from which an estimate of the corresponding streamwise length scale is readily obtained by multiplication with an appropriately chosen convective velocity. A cautious value of the mean convective velocity in the viscous layer at $y^+ = 5$ is about $10u_\tau$, see reference [37], whereas at the other two locations the local mean velocity can be used, and it is about 9, and 15 time u_τ. An estimation of the length scales can be then derived as $\lambda_x^+ = u_c^+ T^+$. We warn the reader that these estimates are very approximate and entirely meant to be used as an indication of the streamwise extent of the structures whose

signature is detected by the shear stress probe. As a general feature, we observe that the largest values of the coherence function are found at low frequencies, i.e. for large scale features of the near wall flow, whereas the coherence drops significantly for large reduced frequencies, i.e. small scale structures. This motivates the observation that large scale features of the near-wall flow are not only those responsible for the largest contribution to the production of turbulence, but also have the most coherent signature on the wall.

The coherence levels are higher near the wall, and decay as the distance is increased. In the viscous sublayer, values in excess of 0.9 are measured at low frequencies. In the buffer layer, at $y^+ = 12$, the coherence is also quite large, but it then decays considerably for the largest distance reported, at $y^+ = 50$.

As figure 11 shows, the coherence function decays quickly for increasing reduced frequencies. In particular, the decay occurs earlier for larger distances from the wall, presumably because fluctuations at small scales compared to the distance probe-wall have very weak signature. By defining as f_0^+ the frequency at which the coherence function is half of the maximum value, as a characteristic measure of the scale where fluctuations are uncorrelated, we obtain for $y^+ = 5$ a value of $T_0^+ = 1/f_0^+ = 14$ to which associate a characteristic length $\lambda_{x_0}^+ = u_c^+ T_0^+ \approx 140$. For $y^+ = 12$, this same quantity is of the order of 300, and the coherence is practically zero at $f^+ = 0.14$, corresponding to scales on the order of 70 viscous units. Therefore, obtaining an accurate estimation in this band is questionable and it appears clear that the focus of the estimation should be on the large scale structures which dominate the buffer layer dynamics.

For the larger distance from the wall, the coherence values are generally lower, and the quantity $\lambda_{x_0}^+$ is of the order of 2000. This is quite a large value, possibly larger than the typical scale of the near wall structures. The reason is that the value of T_0^+ is not derived from the auto-correlation function, from which a more accurate value of the local integral time scale can be obtained. Instead, in our definition, it is derived from the concept of uncorrelation between velocity and wall shear stress fluctuations, as discussed above.

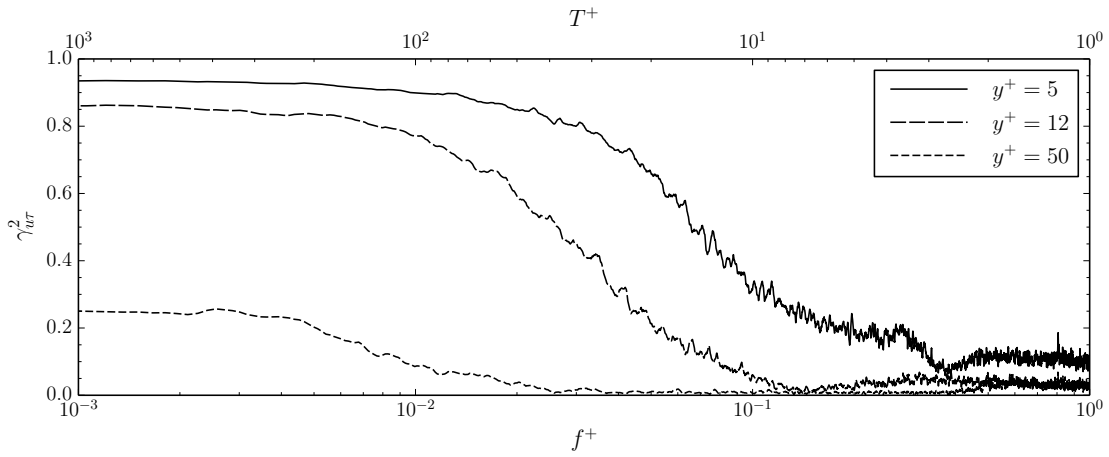

Fig. 11 Squared coherence function of the velocity and wall shear stress fluctuations for three distances from the wall, as a function of the reduced frequency, bottom x-axis scale, or reduced period, top scale.

3. Linear and nonlinear single-time-delay stochastic estimation

For the turbulent channel flow data, the JPDFs for the three distances from the wall are reported in panels (a), (b) and (c) of figure 12. In these figures, selected contours of the JPDFs $p(\tau^*, u^*)$ of the normalized shear stress and velocity fluctuations are shown, where the normalization is such that the velocity and shear stress signal have been normalized with their root-mean-square value, so that all the signals have unit variance. In addition, $p(\tau^*, u^*)$ is normalized so that its integral is equal to one. In light of the discrete nature of the data, this is actually enforced in a discrete fashion. Contours of the JPDF are reported for 1/100, 6/100 and 25/100 for $y^+ = 5$ in panel (a), and for 1/100, 6/100, 15/100 for the two larger distances from the wall. On the same three panels, the conditional averages of the velocity fluctuations are shown as black dots for 10 equally spaced events. The event is defined when the shear stress fluctuation τ^* is within a small window of size $\delta\tau^* = 0.1$ around the event mean value, which ranges from $\tau^* = -2$ to 3. The error bars on the conditional average data represent the conditional root-mean-square value of the velocity fluctuations around the conditional average, and qualitatively represent the size of the uncertainty associated to an estimation using the conditional average. Note that the plots in panels (a), (b) and (c) should be read with τ^* as the independent variable from which u^* is estimated.

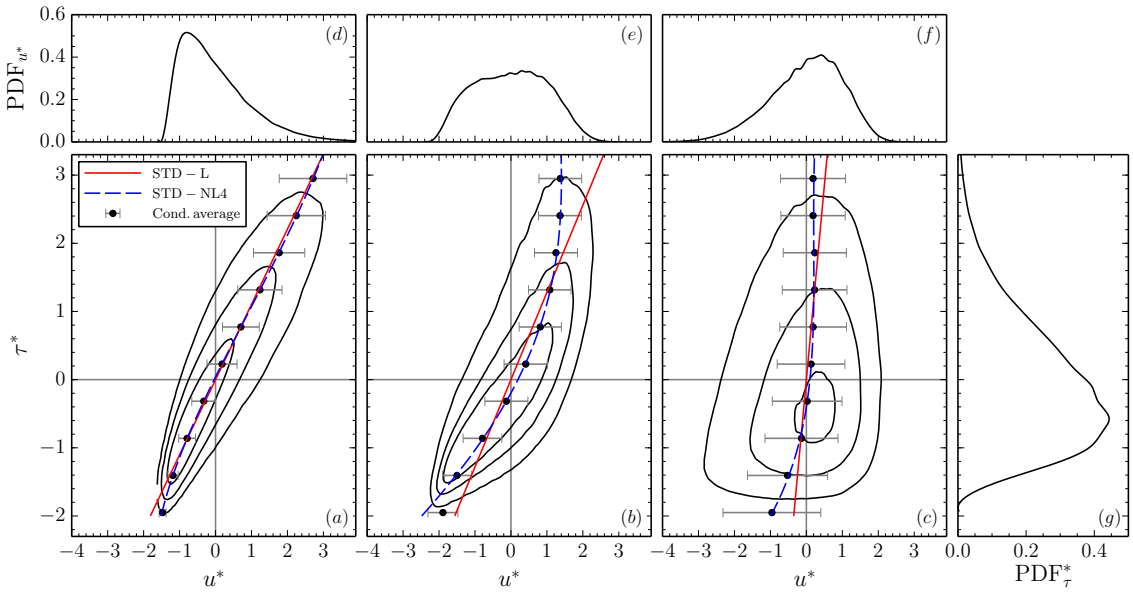

Fig. 12 The central panels show the joint probability density functions $p(\tau^*, u^*)$ of the wall shear stress and of the velocity fluctuation at the three distances from the wall; (a): $y^+ = 5$, (b): $y^+ = 12$, (c): $y^+ = 50$. In the same panels the conditional average and the estimation of the velocity fluctuations with a linear and a nonlinear single-time-delay stochastic technique are reported. The three top panels show the probability density functions of the velocity fluctuations, whereas panel (g) shows the PDF of the wall shear stress fluctuations.

On the same plots, two single-time-delay estimations corresponding to a linear analysis, denoted by STD-L in the legend, and to a fourth order nonlinear technique, denoted as STD-NL4, have also been reported. In addition, panels (d), (e) and (f) of the same figure report the probability density functions of the velocity fluctuations at the three distances, while panel (g) shows the probability density function of the normalized shear stress fluctuations.

The results of figure 12 clearly show that the PDF of the velocity and shear stress fluctuations are significantly far from the Gaussian distribution, in particular for the shear stress and for the data in the viscous layer, panels (g) and (d), respectively, whose marginal distributions exhibit long positive tails, with a markedly negative value of the skewness. However, despite the strong asymmetry of the marginal distributions, the joint distribution is very well represented by a linear behavior. This is evident by how the data points of the conditional average are well approximated

by the linear estimate, with a negligible influence of adding the higher order terms. This indicates that linear estimates are accurate and reliable in this region. The strong linearity in the viscous layer was expected, but it is interesting to observe that the linear relationship continues to hold for large positive events, where the shear stress is large, even though with a lower degree of accuracy as indicated by the longer error bars in this range.

In the buffer layer, at $y^+ = 12$, panel (b), a clear loss of linear behavior is observed. The deviation from linearity is especially strong for large positive and negative values of the shear stress fluctuations: a linear estimate will over/under predict the velocity fluctuation for positive/negative large events. On the other hand, the nonlinear fourth-order estimate more faithfully captures the underlying peculiar property of the JPDF, and as a consequence, it will perform better than a simple linear analysis. The result reported in panel (b) is important in the sense that it is a clear indication that nonlinear estimation techniques should be preferred over simpler linear methods, when the reconstruction of the unsteady flow in the near-wall region is the ultimate aim. This is aggravated by the fact that the improvement is larger for large positive events of the wall shear stress.

For the data at $y^+ = 50$, panel (c), we observe that the contours of the JPDF are now much more rounded and less concentrated around the conditional average data points, which no longer reliably represent in reliable way the joint fluctuations of the shear stress and streamwise velocity. This is better highlighted by the relatively longer error bars around the conditional average data points, with respect to the other two cases at lower y^+, which in turn reflects the general lower values of the cross-correlation coefficient. Nevertheless, results at this distance from the wall are qualitatively similar to those for $y^+ = 12$, with a slight nonlinear behavior underlying the joint distribution of the fluctuations. This appears to indicate that the strong nonlinearity is a feature of the entire buffer and log layers.

The higher accuracy of the nonlinear reconstruction can be quantified by examination of the normalized estimation error ϵ, reported in table 2 as a function of the order d of the single-time-delay stochastic estimation, for the three distances from the wall. Orders up to four are represented since the normalized error then reaches an asymptotic value and little gain is obtained by increasing the

expansion order further. The data essentially reflect the considerations highlighted previously. In the viscous sublayer, accurate reconstructions can be performed by linear approaches, with a total reconstruction of the variance of the velocity fluctuations which exceeds eighty percent. Nevertheless, the accuracy decreases as the distance from the wall increases, and the normalized mean square error reaches 0.32 and 0.96, at $y^+ = 12$ and 50, respectively. On the other hand, the nonlinear techniques perform much better than a linear approach in the buffer layer, because of the strong nonlinearity of the velocity/shear stress coupling in this region.

y^+	$d=1$	$d=2$	$d=4$
5	0.179	0.179	0.176
12	0.389	0.324	0.321
50	0.969	0.960	0.958

Table 2 Normalized mean square estimation error of the velocity fluctuations as a function of the Taylor expansion order for the single-time-delay stochastic estimation, for the three distances from the wall.

Since single-time-delay stochastic estimation relies on information at a single temporal instant, it is clear that using the most correlated sample can result in a more accurate prediction. This is especially the case for convective flows, like the wall-bounded turbulence case considered in the present paper, where the spatial distribution of the coherent structures is embedded in temporal information in the wall sensor signal. The geometric interpretation of this time-delayed stochastic estimation is the same as for standard stochastic estimation, with the exception that the joint probability density function of the fluctuations $u(t)$ and $\tau(t + s\Delta t)$ is of interest. Crucially, the accuracy of single-time-delay stochastic estimation approach now depends on how well these JPDFs are concentrated around the conditional averages of the fluctuations $u(t)$ and $\tau(t + s\Delta t)$, which is summarized by the numerical value of ϵ. In figure 13 the normalized mean square error is reported for the three distances from the wall, in panels (a), (b) and (c), as a function of the shift s. A negative/positive value of s indicates that a past/future samples of the time history of $\tau(t)$ is used. In addition, the top horizontal scale reports the shift in viscous time units. The curves refer to the linear stochastic estimation, $d = 1$ and to nonlinear stochastic estimations, $d = 2, 4$.

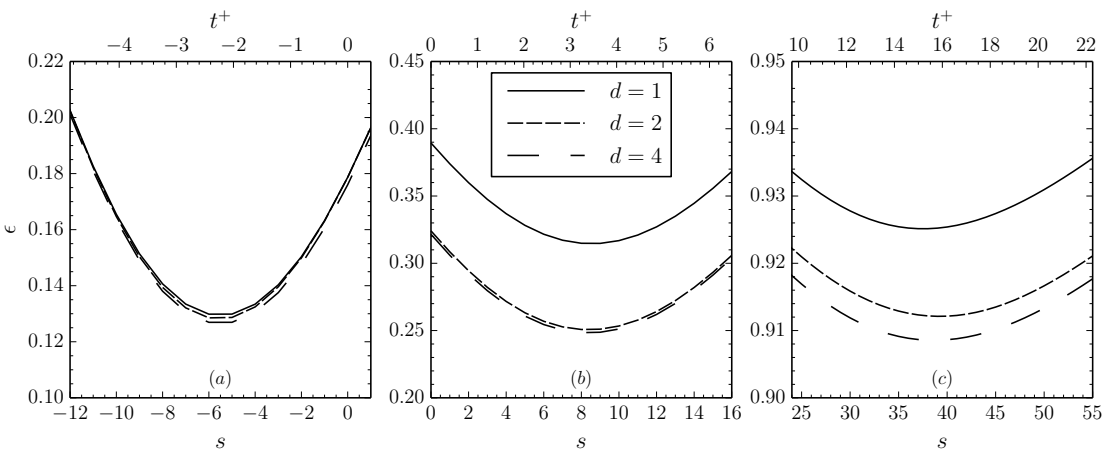

Fig. 13 Normalized mean square error ϵ as a function of the shift s for the three distances from the wall, $y^+ = 5$ in (a), $y^+ = 12$ in (b) and $y^+ = 50$ in (c). The parameter d is the Taylor expansion order as in equation (2).

The general trend, as expected, is that the accuracy of the single-time-delay technique improves when the most correlated sample is used. This occurs for a negative shift for $y^+ = 5$ and for positive shifts for the other two distances, as observed in figure 10. In particular, for the linear case, straight-forward application of the least square method, not reported here, shows that the error of the estimate is minimum when the most correlated samples is used. For the nonlinear case, the same procedure applies, but the minimum value of the error involves high-order moments of the fluctuations, so the optimal shift is different from that for which correlation is maximum.

4. Linear and nonlinear multi-time-delay stochastic estimation

At its core, the linear multi-time-delay technique combines present and past measurements of the wall-mounted sensors and produces a prediction of the flow state that is optimal from the standpoint of the residual error. It is thus interesting, and it is one of the goals of this paper, to understand if the additional information contained in the past samples can be used to improve the prediction for wall-bounded turbulence. Due to the particular configuration of the experimental setup, where the two probes were located at the same streamwise position, the most correlated sample of the wall shear stress time history occurs in the future, introducing a causality issue in the estimation problem. As anticipated, a more convenient, and logical configuration can be imagined, whereby

the sensor is located upstream of the region where state information is required, for example a short distance upstream of the location of wall-mounted actuators, in a feedback control situation.

Nevertheless, in this paper, with the aim of showing the features of the multi-time-delay technique applied to the wall-bounded turbulence problem, we adopt the following approximation. As done for the time-delayed case of figure 13, we artificially shift the time history of the wall shear stress backward or forward with respect to that of the velocity fluctuation, by a quantity s_d, and we then apply the multi-time-delay algorithm on this shifted data set. From a conceptual point of view, this is equivalent to designing a non-causal filter, where past and future samples are used to predict the flow state at the current time. However, we prefer to view this operation from a more physical and pragmatic point of view. In particular, it may be argued that applying the estimation algorithm on a velocity time history shifted backward in time is conceptually analogous to estimating the flow state at a position downstream of the wall sensor. The new position of the velocity sensor can be approximated by $u_c^+ t_d^+$, where u_c^+ is the mean convective velocity at the distance from the wall considered and t_d^+ is the shift expressed in wall units. The validity of this approach is related to the validity of Taylor's hypothesis in near-wall flow, based on the idea that the dominant coherent structures, the estimation of which is the key objective, do not vary much along the short distance $u_c^+ t_d^+$.

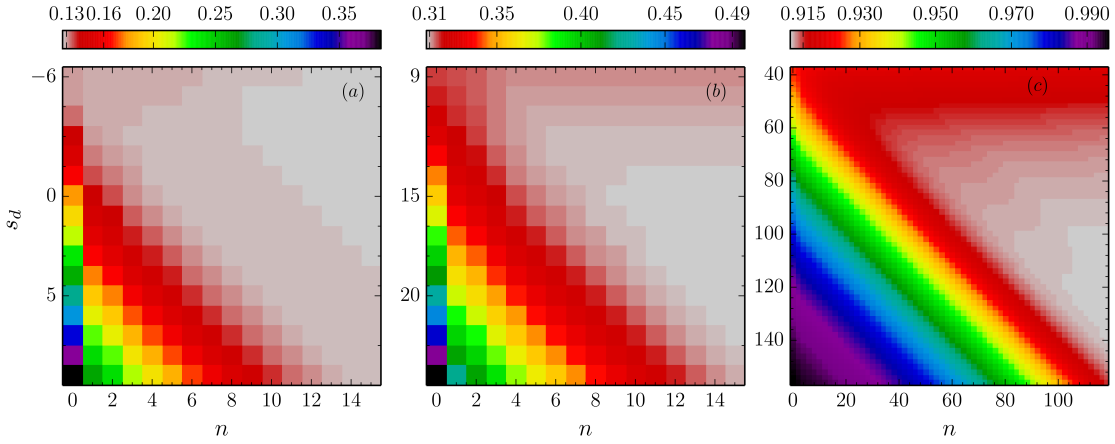

Fig. 14 Normalized mean square error ϵ for multi-time-delay stochastic predictions as a function of n and of the shift s_d for the three distances from the wall, $y^+ = 5$ in (a), $y^+ = 12$ in (b) and $y^+ = 50$ in (c).

Figure 14 shows the behavior of the mean square error ϵ as a function of the shift s_d and n. Results for $y^+ = 5, 12, 50$ are reported in panels (a), (b) and (c) respectively. The color maps have a inherent discrete nature, due to the discrete sampling of the data. The results have been reported with a qualitative color scale, that changes for the three figures, in order to highlight small variations of ϵ around the minimum value, where the color changes from red to gray for small variations of the error. The s_d scales ranges from the value where $\epsilon(n = 0, s_d)$ is minimum, obtained from the minima of the curves in figure 13 for $d = 1$, up to a value of s_d for which the underlying behavior can be identified.

There is a general important trend underlying the three cases: when the shift s_d is that for which $\epsilon(n = 0, s_d)$ is minimum, i.e. $s_d = -6, 8, 37$ respectively, then the reduction in error due to a multi-time-delay approach, so for increasing n is negligible, and certainly not as large as it occurred for the shear layer case discussed previously. This motivates a related observation. By drawing hypothetical lines of constant $\epsilon(n, s_d)$ on the range indicated by the figures, we would observe that on the lower left of the figures these contours would be almost straight, with a slope approximately equal to 1. As a consequence, for a shift s_d larger than the optimal, when past samples are included in the estimation process, the error shows a reduction which stops when the most correlated sample is included. This means that, for instance for $y^+ = 5$, there is no large difference in error for the optimally shifted time-delayed single-time-delay stochastic estimation at $\epsilon(n = 0, s_d = -6)$ and a multi-time-delay stochastic estimation $\epsilon(n = 8, s_d = 4)$. A similar feature is observed for the two larger distances, although there exists some variation, although exaggerated by the rapid variation of the color scale. For a more quantitative analysis, table 3, reports the values of $\epsilon(n, s_d)$ for the two families of linear techniques.

case (linear)	$y^+ = 5$ - $(n,\ s_d)$	$y^+ = 12$ - $(n,\ s_d)$	$y^+ = 50$ - $(n,\ s_d)$
STD	0.130 (0, -6)	0.315 (0, 9)	0.925 (0, 38)
MTD	0.127 (15, -3)	0.308 (15, 19)	0.914 (50, 74)

Table 3 Normalized mean square error ϵ for linear single- and multi-time-delay approaches.

The main result of this comparison can be summarized with the statement that a time-delayed single-time-delay technique, where the most appropriate sample of the shear stress time history is

used, performs equally well, at least from the point of view of the mean square error, than a more elaborate multi-time-delay approach, where appropriate values of s_d and n are used. This statement is more applicable for small distances from the wall, because the improvement of the multi-time-delay technique is slightly larger in the buffer layer, although it is so small that is does not changes the essence of the statement.

From a physical point of view, it can be argued that the interaction between the near-wall structures and their signature on the wall is essentially "static" or scale independent. Once the most appropriate shift is introduced to the wall-shear stress signal, then the prediction of a single-time-delay technique already contains most of the dynamics of the flow field.

Since the relationship between the velocity fluctuations in the buffer layer and the associated shear stress fluctuations at the wall exhibits a significant nonlinear behavior, a comparison between nonlinear single and multi-time-delay, with appropriate shifts in the data, was performed. Due to the relatively large number of past samples that has to be included in the estimation process we decided to develop the nonlinear filter as a feed-forward neural network, rather than using a model based on a Volterra series, to make the problem computationally solvable. In addition, because the training process is an expensive and lengthy process, we did not evaluate the accuracy of the nonlinear approach for all the combinations of s and n as done for the linear case in figure 14. By contrast, with the aim of understanding the basic behavior we selected one pair (n, s) to test the nonlinear approach, based on the results of figure 14. These combinations of n and s_d are the same as those reported in table 3.

For these analyzes we used neural networks with a single hidden layer, and with a number n_h of nodes equal to 10 for the cases at $y^+ = 5$ and 12, and with an increased value of 20 for $y^+ = 50$, in reason of the larger value of input samples. Since the training of the neural network is a non-convex optimization problem [24], possibly affected by the presence of several local minima, we repeated the training process three times and we selected the network with the lowest mean square error. Typically, training was stopped when the first four significant digits of the mean square error were converged. Although the results reported here were obtained from estimators trained on the entire dataset, we have performed extensive preliminary analyzes to exclude the occurrence of over-fitting

problems. As an example, for the nonlinear estimator at $y^+ = 50$, the most critical since it has the largest number of tunable parameters, the relative difference between the errors on the training and validation sets was lower than 1/1000. For all the other estimators, including the linear estimators of figure 14, the relative difference was even smaller, or on the same order of magnitude.

case (nonlinear)	$y^+ = 5$ - $(n,\ s_d)$	$y^+ = 12$ - $(n,\ s_d)$	$y^+ = 50$ - $(n,\ s_d)$
STD	0.127 (0, -6)	0.248 (0, 8)	0.909 (0, 39)
MTD	0.125 (15, -3)	0.237 (15, 19)	0.903 (50, 74)

Table 4 Normalized mean square error ϵ for nonlinear single- and multi-time-delay approaches.

Results of this investigation are reported in table 4, which also contains the numerical values of the mean square error for the nonlinear single-time-delay approach with expansion order $d = 4$, with optimal shift applied to the shear stress time history. We clearly observe that the improvement in accuracy of the nonlinear multi-time-delay approach, with respect to the single-time-delay nonlinear technique is marginal. This result appears to corroborate the comments offered for the linear approaches, which can be summarized with the fact that the interaction between the near-wall coherent structures and the wall itself is essentially "static" or scale independent and, at its core, "memoryless".

The accuracy of the different techniques, summarized by the normalized mean square error, can also be assessed in the frequency domain, to highlight the frequencies, or length scales, where accumulation of estimation error occurs. We choose to report the comparison by reporting the behavior of the quantity η, defined as

$$\eta(f^+) = \frac{\Phi_{e_{\{\cdot\}}}(f^+)}{\Phi_{e_{STD-L}}(f^+)} \tag{10}$$

where $\Phi_{e_{STD-L}}$ is the power spectral density of the estimation error time series associated with the linear single-time-delay technique, while $\Phi_{e_{\{\cdot\}}}$ stands for the spectral density of the error time series corresponding to the other three techniques investigated in the paper. The parameters for the techniques are the same as for the results reported in tables 3 and 4. For a given technique, a value of $\eta(f^+)$ lower than one indicates that technique is more accurate than a linear single-time-delay approach at that frequency.

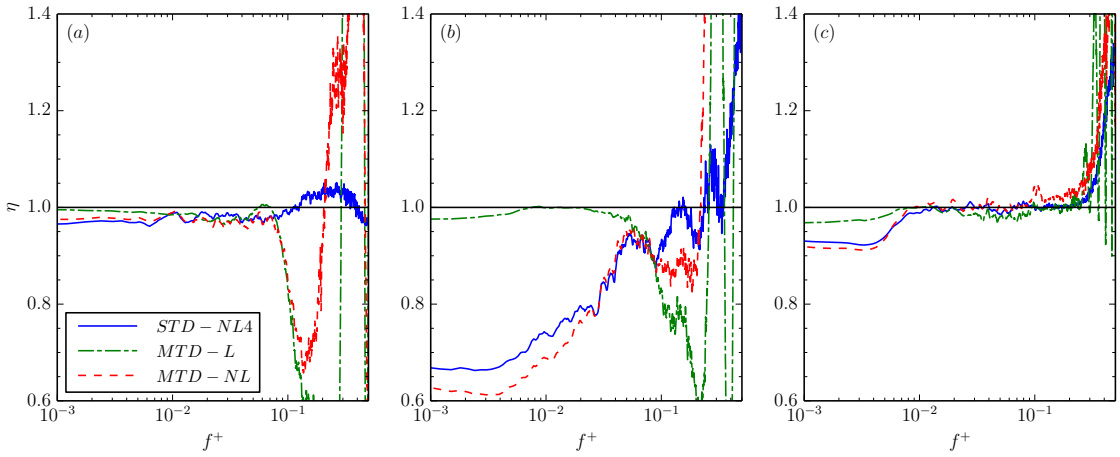

Fig. 15 Ratio between the power spectrum of the estimation error of the linear time-delayed single-time-delay technique and those related to the other approaches as reported in tables 3 and 4. (a) **:** $y^+ = 5$**,** (b) **:** $y^+ = 12$**,** (c) **:** $y^+ = 50$**.**

The result of these analyzes is reported in figure 15, which shows the behavior of η for the three distances from the wall. In the viscous layer, panel (a), we observe that the four approaches have essentially the same performances below $f^+ = 10^{-1}$, where most of the energy of the fluctuation is concentrated, and with little difference between the linear and nonlinear techniques. Differences arise for $f^+ > 10^{-1}$, in particular for the multi-time-delay approaches. In fact, we observe that both the linear and nonlinear multi-time-delay techniques produce estimates with lower error with respect to the reference technique in this range, and also with respect to the nonlinear single-time-delay technique. This difference, responsible for the slight reduction in estimation error, is more important from a fundamental point of view, because it is a restatement of the property that multi-time-delay approaches are able to retain only the coherent components, filtering noise and uncorrelated motions. We also observe that at very large frequencies the two multi-time-delay techniques produce quite a large error with respect to the linear single-time-delay approach. This is essentially due to the fact that causality of the problem is not completely recovered. In fact, tests not reported here show that by increasing the value of the shift s_d between the time histories, and the value of n accordingly, this high frequency noise is removed.

In the buffer layer, panel (b), we observe that for the linear multi-time-delay technique the value of η lies around one for most of the frequency range associated with large scale coherent structures,

and decays only somewhere around $f^+ \approx 0.08$, with the high-frequency behavior similar to what discussed for the viscous layer. On the other hand, we observe that the two nonlinear techniques produce very similar results, with a slightly lower error for the multi-time-delay case, and give a much more reliable estimate of the velocity fluctuations associated to the large scale motions as extensively discussed in the paper. However, the improvement with respect to the linear techniques appears to vanish from frequencies above $f^+ = 0.08$.

Finally, the results for $y^+ = 50$ indicate that there is not a large difference between the four techniques discussed, even though the error for the two nonlinear techniques is slightly lower at very low frequencies, where some degree of nonlinearity in the relation between the velocity and shear stress fluctuations is detected.

V. Conclusions

In this paper a nonlinear extension of the multi-time-delay stochastic estimation technique was introduced and results of its application to two significantly different flows were presented and discussed. The estimation of a cavity shear layer from wall-pressure measurements and the estimation of the streamwise velocity in the near-wall region of a turbulent channel flow at $Re_\tau = 180$, based on shear stress measurements, were chosen as test cases. The proposed nonlinear technique is based on Volterra series expansions, for problems where a limited number of samples is required, or on Artificial Neural Networks when the estimation problem is characterized by an higher dimensionality, i.e. for strong nonlinear behavior or when a large number of past samples has to be included.

The improvement in terms of normalized mean-square estimation error, over the linear multi-time-delay technique is found to be very marginal for the cavity shear layer case, which offers in turn a drastic improvement over classical linear and nonlinear single-time-delay techniques. In this case, the intrinsic nonlinearity in the data appears small and energetically not very relevant. It can be argued that for the cavity flow this may be due to the fact that the velocity fluctuations are forced by the acoustic resonance of the wind tunnel facility, and that they have saturated to a large value so that nonlinear effects have small influence. This hypothesis requires further verification, since other authors have reported quite significant improvements when using nonlinear techniques. Nevertheless, we highlighted a fundamental feature of the nonlinear technique. In fact, it was shown

that by using such an approach it is possible to accurately reconstruct complex spectral features, which cannot be obtained for a purely linear approach. In particular, it was shown that all the integer multiples of the fundamental oscillation frequency of the velocity signal were recovered, and not only those for which large values of the coherence function were observed. In addition, we showed that despite the fact that both the single and multi-time delay nonlinear techniques possess this feature, the improvement was larger for the multi-time-delay technique, which provided a better control of the amplitude of the reconstructed peaks. The improvement was slight in quantitative terms but from a qualitative point of view it is what makes the nonlinear multi-time-delay technique appealing. Results for the turbulent channel flow are more encouraging from a quantitative point of view. First of all, we observed that in the region closer to the wall, in the viscous layer, a linear method provides a faithful representation of the flow state. On the other hand, and especially in the buffer layer, inclusion of the nonlinear terms is required. In particular, the reduction of the estimation error when these terms are included is due to a better reconstruction at frequencies corresponding to the most important large scale coherent structures in the buffer layer, which have a strong nonlinear character. A second important conclusion is that multi-time-delay techniques do not result in a more reliable estimation with respect to a single-time-delay technique when the most correlated sample in used. From a physical point of view, this means that, at least from the standpoint of the reconstruction error, the interaction between the near-wall structures and the wall is essentially static, or scale independent. From a practical point of view, this result appears to indicate that simpler single-time-delay techniques could be used for the estimation problem, although they might be less robust to contaminating noise sources.

To summarize, a further important conclusion drawn in this paper is that the improvement in accuracy brought by the nonlinear technique is application dependent, as nonlinear phenomena may or may not be energetically relevant for the problem at hand. On this point, the improvement may not be significant in terms of normalized mean-square error but it may be important from the point of view of the recovery of complex spectral details. Secondly, it has to be remarked that the improvement in accuracy may not be worth the additional complexity and the associated increased computational costs of the nonlinear technique, especially if real-time control of fluid flows is of

interest. A related note is that Volterra series expansion may be preferred for small problems, since the optimization problem involved is convex and relatively faster than the non-convex training process of neural networks. Furthermore, a better control on the nonlinearity of the estimation technique is reasonably guaranteed by such an approach. On the other hand, neural networks have the remarkable advantage of having a lower complexity, and the associated nonlinear estimation problem is tractable also when the dimensionality or the nonlinearity of the data is large.

VI. Acknowledgments

The scholarship Ernesto e Ben Omega Petrazzini, from Accademia delle Scienze di Torino, to support the work of Ms Linda Fronges, is gratefully acknowledged.The first author gratefully acknowledges the financial support of AIDAA and of the University of Southampton for the participation to the AIAA SciTech 2014 conference where a preliminary version of this manuscript was presented.

[1] Colburn, C. H. and Cessna, J. B. and Bewley, T. R., "State estimation in wall-bounded flow systems. Part 3. The ensemble Kalman filter," *Journal of Fluid Mechanics*, Vol. 682, 2011, pp. 289-303, doi:10.1017/jfm.2011.222

[2] Adrian, R. J., "On the role of conditional averages in turbulence theory," *Turbulence in Liquids*, Vol. 1, 1977, pp. 323-332.

[3] Clark, H. and Naghib-Lahouti, A. and Lavoie, P., "General perspectives on model construction and evaluation for stochastic estimation, with application to a blunt trailing edge wake," *Experiments in Fluids*, Vol. 55, No. 7, 2014, pp. 1-19, doi:10.1007/s00348-014-1756-y

[4] Ewing, D. and Citriniti, J. H., "Examination of a LSE/POD complementary technique using single and multi-time information in the axisymmetric shear layer," *IUTAM Symposium on simulation and identification of organized structures in flows*, 1999, pp. 375-384, doi:10.1007/978-94-011-4601-$2_3$3

[5] Tinney, C. E. and Coiffet, F. and Delville, J. and Hall, A. M. and Jordan, P. and Glauser, M.N., "On spectral linear stochastic estimation," *Experiments in fluids*, Vol. 41, No. 5, 2006, pp. 763-775, doi:10.1007/s00348-006-0199-5

[6] Ukeiley, L. and Murray, N. and Song, Q. and Cattafesta, L., "Dynamic surface pressure based estimation for flow control," *IUTAM Symposium on Flow Control and MEMS*, Vol. 1, 2008, pp. 183-189, doi:10.1007/978-1-4020-6858-$4_2$1

[7] Durgesh, V. and Naughton, J. W., "Multi-time-delay LSE-POD complementary approach applied to unsteady high-Reynolds-number near wake flow," *Experiments in fluids*, Vol. 49, No. 3, 2010, pp. 571-583, doi:10.1007/s00348-010-0821-4

[8] Lasagna, D. and Orazi, M. and Iuso, G., "Multi-time delay, multi-point linear stochastic estimation of a cavity shear layer velocity from wall-pressure measurements," *Physics of Fluids (1994-present)*, Vol. 25, No. 1, 2013, pp. 017101, doi:10.1063/1.4774337

[9] Naguib, A. M. and Wark, C. E. and Juckenhöfel, O., "Stochastic estimation and flow sources associated with surface pressure events in a turbulent boundary layer," *Physics of Fluids (1994-present)*, Vol. 13, No. 9, 2001, pp. 2611-2626, doi:10.1063/1.1389284

[10] Hudy, L. and Naguib, A. M. and and Humphreys, W. M., "Stochastic estimation of a separated-flow field using wall-pressure-array measurements", Physics of Fluids (1994-present), 19.2, 2007, 024103

[11] Baars, W. J., and Charles E. T., "Proper orthogonal decomposition-based spectral higher-order stochastic estimation," *Physics of Fluids (1994-present)*, Vol. 26, No. 5, 2014, pp. 055112, doi:10.1063/1.4879255

[12] Buffoni, M. and Camarri, S. and Iollo, A. and Lombardi, E. and Salvetti, M. V., "A non-linear observer for unsteady three-dimensional flows," *Journal of Computational Physics*, Vol. 227, No. 4, 2008, pp. 2626-2643, doi:10.1016/j.jcp.2007.11.005

[13] Narayanan, S., Khibnik, A. I., Jacobson, C. A., Kevrekedis, Y., Rico-Martinez, R., & Lust, K., "Low-dimensional models for active control of flow separation", In Control Applications, Proceedings of the 1999 IEEE International Conference on (Vol. 2, pp. 1151-1156), 1999

[14] Siegel, S. G. and Seidel, J. and Fagley C. and Luchtenburg, D. M., Cohen, K. and McLaughlin, T. "Low-dimensional modelling of a transient cylinder wake using double proper orthogonal decomposition", Journal of Fluid Mechanics, 610, 2008, pp. 1-42 doi:10.1017/S0022112008002115

[15] Gillies, E. A., "Low-dimensional control of the circular cylinder wake", Journal of Fluid Mechanics, 371(1), 157-178, 1998

[16] Samimy, M. and Debiasi, M. and Caraballo, E. and Malone, J. and Little, J. and Ozbay, H. and ... & Camphouse, R. C. "Exploring strategies for closed-loop cavity flow control", AIAA paper, 576, 2004

[17] Lee, C. and Kim, J. and Babcock, D. and Goodman, R., "Application of neural networks to turbulence control for drag reduction", Physics of Fluids (1994-present), 9, 1740-1747, 1997, doi:10.1063/1.869290

[18] Cohen, K., Siegel, S., Seidel, J., Aradag, S., & McLaughlin, T., "Nonlinear estimation of transient flow field low dimensional states using artificial neural nets", Expert Systems with Applications, 39(1), 1264-1272, 2012

[19] Murray, N. E. and Ukeiley, L., "Modified quadratic stochastic estimation of resonating subsonic cavity flow," *Journal of Turbulence*, Vol. 8, 2007, doi:10.1080/14685240701656121

[20] Zhang, K. and Naguib, A. M., "Effect of finite cavity width on flow oscillation in a low-Mach-number cavity flow," *Experiments in fluids*, Vol. 51, No. 5, 2011, pp. 1209-1229, doi:10.1007/s00348-011-1142-y

[21] Guezennec, Y.G.,"Stochastic estimation of coherent structures in turbulent boundary layers," *Physics of Fluids A: Fluid Dynamics (1989-1993)*, Vol. 1, No. 6, 1989, pp. 1054-1060, doi:10.1063/1.857396

[22] Bewley, T. R. and Protas, B., "Skin friction and pressure: the "footprints" of turbulence," *Physica D: Nonlinear Phenomena*, Vol. 196, No. 1, 2004, pp. 28-44, doi:10.1016/j.physd.2004.02.008

[23] Pitas, I. and Venetsanopoulos, A. N., "Nonlinear digital filters: principles and applications", Vol. 84, Springer, 1990.

[24] Haykin, S., "Neural networks: a comprehensive foundation", Prentice Hall PTR, 1994.

[25] Hastie, T., Tibshirani, R., Friedman, J., Hastie, T., Friedman, J., & Tibshirani, R., "The elements of statistical learning", 2009, Springer

[26] Lasagna, D. and Donelli, R. and De Gregorio, F. and Iuso, G., "Effects of a trapped vortex cell on a thick wing airfoil," *Experiments in fluids*, Vol. 51, No. 5, 2011, pp. 1369-1384, doi:10.1007/s00348-011-1160-9

[27] Donelli, R. and Iannelli, P. and Chernyshenko, S. and Iollo, A. and Zannetti, L. and others, "Design and analysis of vortex cells," *AIAA Journal*, Vol. 47, No. 2, 2009, pp. 451-467, doi:10.2514/1.37662

[28] Tutty, O. and Savelsberg, R. and Castro, I. P., "Three-dimensional flow in circular cavities of large spanwise aspect ratio," *Journal of Fluid Mechanics*, Vol. 707, 2012, pp. 551-574, doi:10.1017/jfm.2012.301

[29] Chatellier, L. and Laumonier, J. and Gervais, Y. "Theoretical and experimental investigations of low Mach number turbulent cavity flows," *Experiments in fluids* Vol. 36, No. 5, 2004, pp. 728-740, doi:10.1007/s00348-003-0752-4

[30] Sipp, D. "Open-loop control of cavity oscillations with harmonic forcings," *Journal of Fluid Mechanics*, Vol. 708, 2012, pp. 439-468, doi:10.1017/jfm.2012.329,

[31] Samimy, M. and Debiasi, M. and Caraballo, E. and Serrani, A. and Yuan, X. and Little, J. and Myatt, J. H., "Feedback control of subsonic cavity flows using reduced-order models", Journal of Fluid Mechanics, 579, 2007: 315-346.

[32] Bendat, J. S. and Piersol, A. G. "Random data: analysis and measurement procedures", Vol. 729, John Wiley & Sons, 2011.

[33] Brereton, G. J., "Stochastic estimation as a statistical tool for approximating turbulent conditional averages," *Physics of Fluids A: Fluid Dynamics (1989-1993)*, Vol. 4, No. 9, 1992, pp. 2046-2054, doi:10.1063/1.858374

[34] Schoppa, W. and Hussain, F., "Genesis and dynamics of coherent structures in near-wall turbulence - A new look". *Self-sustaining mechanisms of wall turbulence (A 98-17710 03-34), Southampton, United Kingdom, Computational Mechanics Publications(Advances in Fluid Mechanics Series)*, Vol. 15, 1997, pp. 385-422.

[35] Iuso, G. and Onorato, M.and Spazzini, P. G. and Di Cicca, G., "Wall turbulence manipulation by large-scale streamwise vortices," *Journal of Fluid Mechanics*, Vol. 473, 2002, pp. 23-58, doi:10.1017/s0022112002002574

[36] Adrian, R. J. and Meinhart, C. D. and Tomkins, C. D., "Vortex organization in the outer region of the turbulent boundary layer," *Journal of Fluid Mechanics*, Vol. 422, 2000, pp. 1-54, doi:10.1017/s0022112000001580

[37] Quadrio, M. and Luchini, P., "Integral space–time scales in turbulent wall flows,". *Physics of Fluids (1994-present)*, Vol. 15, No. 8, 2003, pp. 2219-2227, doi:10.1063/1.1586273